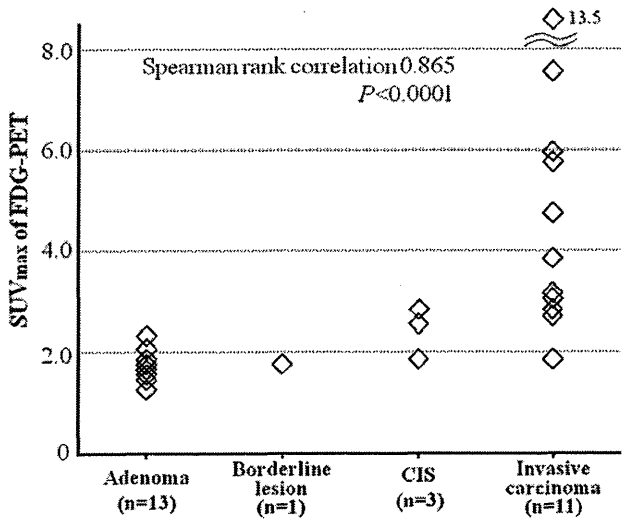

Figure 2. Correlation between histopathological type of IPMN and SUVmax of FDG-PET in 28 patients. Among the enrolled 29 patients, one patient with hyperglycemia at the FDG-PET examination was excluded. For abbreviations, see Fig. 1. SUVmax, maximum standardized uptake value; FDG-PET, 2-[^{18}F] fluoro-2-deoxy-D-glucose positron emission tomography

120 kV, a tube current of 300 mA, and a rotation period of 0.5 sec. Images of 5 mm slice thickness were used for evaluation. Contrast-enhanced multiphasic CT images were acquired at 10 sec after the peak aortic enhancement (arterial phase), followed by pancreatic phase and portal venous phase for upper abdomen. Nonionic contrast medium, 300 mg of iodine per milliliter, was administered intravenously at a rate of 4 ml/sec with a power injector. Images were interpreted especially focusing on the presence of mural nodule as well as the size of tumor and presence of dilatation of main pancreatic duct.

Histopathological diagnosis of IPMN. The diagnosis of IPMN of the pancreas in the enrolled 29 patients was confirmed on histopathological examination of the resected specimens by an experienced pathologist. The lesions were histopathologically classified into the following subtypes: adenoma, borderline lesion, CIS, and invasive carcinoma. Adenoma and borderline lesions were categorized as benign lesions, while CIS and invasive carcinoma were categorized as malignant lesions.

Statistical analysis. Receiver operating characteristic (ROC) curve analysis was performed using sensitivity and specificity at various cut-off values. The significance of differences among the groups was assessed by the χ^2, Fisher's exact test or the Mann-Whitney U test. Statistical analysis was performed using StatView (version 5.0, SAS Institute Inc, Cary, NC). A P-value <0.05 was considered statistically significant.

Ethical considerations. The study protocol was approved by the Human Ethics Review Committee of Osaka University Hospital and a signed consent form was obtained from each patient.

Results

Patient and tumor characteristics. Table I summarizes the clinical characteristics of the included 29 patients with histopathological confirmation. Among 27 patients who underwent ERCP, 9 were diagnosed as malignant IPMN based on pancreatic duct lavage cytology and/or pancreatic juice cytology. Five patients (17.2%) had multiple cystic lesions. Five patients presented with high serum levels of CEA (≥5.0 ng/ml) and 5 patients with high CA 19-9 (≥37 U/ml). The most common location of the lesion was in the head or uncinate of the pancreas (44.8%). Three patients had the main duct type (10.4%), 13 the combined type (44.8%), and 13 the branch type (44.8%). Based on the CT findings, the mean diameter of the cystic lesion was 39 mm (range, 14-75 mm) in patients with combined type and branch type, and the MPD diameter was 11.1 mm (range, 5.0-41.0 mm) in patients with main duct type and combined type. Mural nodules were identified in 13 patients (44.8%). Malignant IPMN was identified in 14 (48.3%) patients, including 11 with invasive carcinoma and 3 with CIS. The remaining 15 patients (51.7%) had benign IPMN: one borderline lesion, and 14 adenomas. The mean SUVmax of FDG-PET of the lesion for all patients was 3.3 (range, 1.3-13.5).

Correlation between histopathological type and SUVmax of FDG-PET. Fig. 2 displays the SUVmax for each histopathological type of IPMN. This analysis was performed in the 28 patients, while the remaining one patient with hyperglycemia at the FDG-PET examination was excluded from this analysis. The SUVmax correlated with the histopathological type (Spearman rank correlation 0.865, P<0.0001). In detail, there were significant differences of the SUVmax between invasive carcinoma and others (CIS, borderline lesion, and adenoma), and between malignant IPMNs and benign IPMNs. Moreover, the SUVmax in patients with CIS was significantly higher than that with benign IPMNs. The following examination focuses on the difference between malignant IPMNs and benign IPMNs.

Comparison of clinical features of patients with benign and malignant IPMN. Table I summarizes the clinical features of patients with benign IPMNs and malignant IPMNs. There was no significant difference in gender, age, the presence of symptoms, serum levels of CEA and CA19-9, multiplicity, location, IPMN type, diameter of the lesion, and MPD diameter between the two groups. On the other hand, the frequency of the presence of mural nodule in malignant IPMN (92.9%) was significantly higher than that in benign IPMN (20.0%, P=0.0001). Furthermore, the SUVmax in patients with malignant IPMNs (4.7±3.0) was significantly higher than that with benign IPMNs (1.8±0.3, P=0.0011).

Comparison of diagnosis of malignant IPMN by FDG-PET and CT. Table II lists the distribution of patients, sensitivity, specificity, and accuracy of FDG-PET and certain CT features of the tumors. Diagnosis of malignancy by FDG-PET was analyzed using various cut-off levels of SUVmax. Moreover, ROC curve was constructed by plotting sensitivity and specificity at various cut-off levels of SUVmax (Fig. 3). Such

Table I. Clinical and histopathological characteristics of the patients with intraductal papillary-mucinous neoplasms (IPMN).

	Histopathological confirmation (+)			Histopathological confirmation (+) (n=29)	Histopathological confirmation (-) (n=43)
	Benign (n=15)	Malignant (n=14)	p-value		
Gender			0.8367		
Male	8	8		16	24
Female	7	6		13	19
Age (years)	64±11	66±9	0.3736	65±10 (48-82)	68±11 (41-90)
Symptom			0.1976		
Present	5	6		11	2
Absent	10	8		18	41
CEA (ng/ml)	2.1±1.0	3.4±3.6	0.1561	2.8±1.9 (1-8)	5.1±12.9 (1-69)
CA19-9 (U/ml)	26.2±21.3	38.3±50.1	0.2118	28.3±48.3 (5-240)	22.1±14.7 (5-60)
Multiplicity			>0.9999		
Solitary	12	12		24	28
Multiple	3	2		5	15
Location			0.4865		
Head or uncinate	6	7		13	19
Body	4	5		9	12
Tail	5	2		7	12
Type			0.5859		
Main duct	1	2		3	1
Combined	6	7		13	9
Branch duct	8	5		13	33
Diameter of cystic lesion (mm)[a]	41±15	36±15	0.3498	39±15 (14-75)	21±14 (2-55)
MPD diameter (mm)[b]	7.6±3.0	13.8±11.9	0.1993	11.1±9.5 (5.0-41.0)	4.8±3.0 (2.1-11.0)
Mural nodule			>0.0001		
Present	3	13		16	6
Absent	12	1		13	37
Cytology[c]			0.0006		
Positive	0	9		9	1
Negative	13	5		18	21
Histopathological type			-		
Adenoma	14	-		14	-
Borderline lesion	1	-		1	-
CIS	-	3		3	-
Invasive carcinoma	-	11		11	-
SUVmax of FDG-PET[d]	1.8±0.3	4.7±3.0	0.0011	3.3±2.6 (1.3-13.5)	1.7±0.6 (1.0-4.4)

[a]Diameter of cystic lesion was determined on CT in patients with combined and branch types. [b]MPD diameter was determined on CT in patients with main duct and combined types. [c]Cytology was performed in 49 patients. [d]Two patients were excluded from analysis of SUVmax for hyperglycemia at the FDG-PET examination. CEA, carcinoembryonic antigen; CA19-9, carbohydrate antigen; MPD, main pancreatic duct; CIS, carcinoma *in situ;* SUVmax, maximum standardized uptake value; FDG-PET, 2-[^{18}F] fluoro-2-deoxy-D-glucose positron emission tomography.

analysis showed that the optimal cut-off level of SUVmax of FDG-PET was 2.5 for differentiation of malignant IPMN. Using this cut-off level, the sensitivity, specificity, and accuracy of differentiation of malignant IPMN were 93,

Table II. Distribution of patients, sensitivity, specificity and accuracy of FDG-PET and certain CT parameters associated with a higher likelihood of malignancy.

		FDG-PET (SUVmax cut-off value)[a]						CT Findings					
		2.0		2.5		3.0		Diameter of cystic lesion (mm)[b]		MPD diameter (mm)[c]		Mural nodule	
	n	(+)	(-)	(+)	(-)	(+)	(-)	≥30	<30	≥7	<7	(+)	(-)
Adenoma	14	2	11	0	13	0	13	11	2	2	4	2	12
Borderline	1	0	1	0	1	0	1	1	0	1	0	1	0
Carcinoma *in situ*	3	2	1	2	1	0	3	1	1	1	2	2	1
Invasive carcinoma	11	11	0	11	0	10	1	6	4	5	1	11	0
Sensitivity (%)		93		93		71		58		67		93	
Specificity (%)		86		100		100		14		57		80	
Accuracy (%)		89		96		86		35		63		86	

[a]In the analysis of the FDG-PET (SUVmax cut-off value) (left side), one adenoma patient with hyperglycemia at the FDG-PET examination was excluded. [b]Diameter of cystic lesion was determined on CT in patients with combined and branch types. [c]MPD diameter was determined on CT in patients with main duct and combined types. FDG-PET, 2-[^{18}F] fluoro-2-deoxy-D-glucose positron emission tomography; SUVmax, maximum standardized uptake value; MPD, main pancreatic duct.

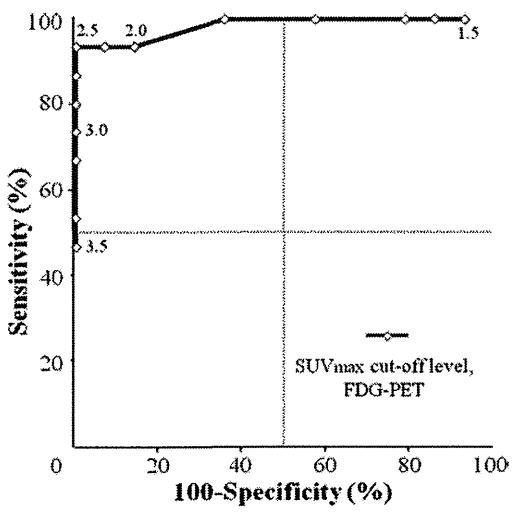

Figure 3. ROC curve for the differential diagnosis of benign IPMN and malignant IPMN according to SUVmax of FDG-PET. Data on the curve represent SUVmax cut-off levels of 1.5-3.5. For abbreviations, see Fig. 1. ROC, receiver operating characteristic.

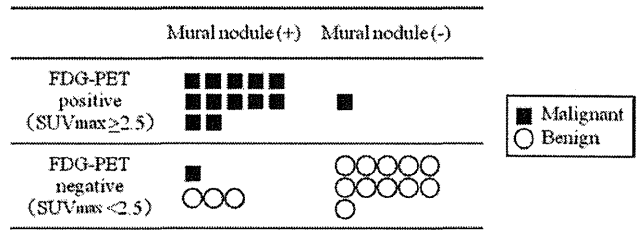

Figure 4. Correlation between histopathological type and results of combination of FDG-PET (SUVmax) and CT (mural nodule) in 28 patients with IPMNs. Among the enrolled 29 patients, one patient with hyperglycemia at the FDG-PET examination was excluded. For abbreviations, see Fig. 1. CT, computed tomography.

100, and 96%, respectively. These values were superior to those of CT parameters that had been reported previously to be associated with a higher likelihood of malignancy (5,9-17), including large cystic lesion size (≥3.0 vs. <3.0 cm), and large dilatation of MPD (≥7 vs. <7 mm) (Table II). In comparison to the presence/absence of mural nodules, which is also previously reported to be associated with malignancy, though the sensitivity was almost equal, the specificity and accuracy were superior (Table II).

Combination of FDG-PET findings and mural nodule in diagnosis of malignancy. Based on the above results, both the FDG-PET findings and the presence/absence of mural nodule on CT were considered useful in differentiation of malignant IPMN. Therefore, the combination of SUVmax of FDG-PET and mural nodule on CT were used for the diagnosis of malignancy (Fig. 4). In this analysis, SUVmax of ≥2.5 was considered positive for malignancy. All patients with SUVmax ≥2.5 and mural nodule were histopathologically confirmed to have malignant IPMN (n=12), and all patients with SUVmax <2.5 and no mural nodule had benign IPMN (n=11). A representative patient with malignant IPMN, positive PET finding and mural nodule is shown in Fig. 5A. In the remaining 5 patients, there was discrepancy in PET findings and presence/absence of mural nodule. Four of the 5 patients had mural nodule on CT scans, but their nodule was negative on FDG-PET. Among the 4 patients, 3 were confirmed to have benign tumors and one had malignant IPMN.

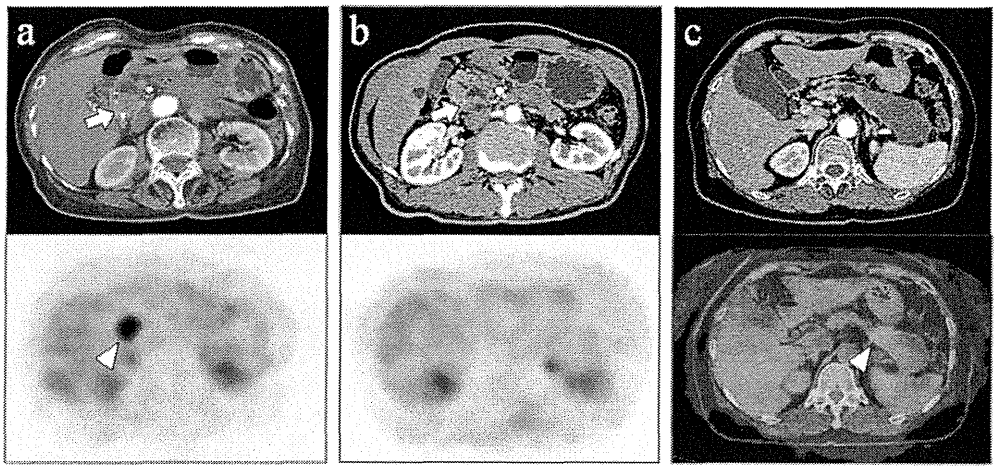

Figure 5. CT and FDG-PET findings of three representative cases [(A) malignant IPMN, (B) benign IPMN, (C) malignant IPMN]. Arrows, mural nodules on CT; arrowheads, the most intense area of FDG accumulation on PET. For abbreviations, see Fig. 1. CT, computed tomography.

The CT and FDG-PET of a representative patient with mural nodule who had negative FDG-PET is shown in Fig. 5B. On the other hand, one patient with malignant IPMN had a positive lesion on FDG-PET (in pancreatic body), but mural nodule could not be identified even on thin-slice CT scans (Fig. 5C).

Follow-up of patients without surgical resection. The clinical characteristics of the 43 patients followed up without surgical resection are also shown in Table I. In 4 of the 43 patients followed up, the SUVmax was ≥2.5. One patient, who had a mural nodule suggesting malignancy with the SUVmax being 4.4, did not undergo surgery because of refusal, but wished to be followed up without any treatment. Now, 10 months after the start of follow-up, the tumor has been gradually increasing and a pulmonary metastasis has identified. In one patient having a mural nodule with the SUVmax being 3.2, who also did not undergo surgery for poor risk and followed-up without any treatment, the tumor has been gradually increasing, now, 24 months after the start of follow-up. In the remaining 2 patients, the tumor had gradually progressed despite chemotherapy, and then they died of the invasive cancer. On the other hand, in the remaining 39 patients with the SUVmax <2.5, the tumor has been unchanged for the follow-up period. The median follow-up period of the 39 patients was 24 months. Under the condition that the histopathological type of IPMN in the patients with growing tumor and the patients with unchanged tumor were hypothesized as malignant and benign, respectively, the sensitivity, specificity, and accuracy of FDG-PET with cut-off level being 2.5 for the differentiation of malignant IPMN were 100, 100, and 100%.

Discussion

In the present study, the sensitivity, specificity, and accuracy of FDG-PET were examined using several cut-off levels of SUVmax to differentiate between benign and malignant IPMN of the pancreas. The results showed that at the optimal cut-off level of SUVmax was 2.5, with the specificity, sensitivity and accuracy being 93, 100 and 96%, respectively. Mansour *et al* (24) previously examined 68 patients with pancreatic cystic tumors and reported that the sensitivity and specificity of PET for malignancy were 57 and 85%, respectively. However, only 5 patients had an IPMN, and since detailed criteria for the positive/negative PET findings were not reported in that study, it is difficult to compare the results of our current study to their study. On the other hand, Sperti et *al* (25) reported that FDG-PET was useful for differentiation of benign and malignant IPMN with the specificity, sensitivity and accuracy of 92, 97 and 95%, respectively, using a cut-off level of SUVmax of 2.5, though it was not clear in their report whether they had investigated the usefulness with any cut-off levels of SUVmax other than 2.5. The results of the present study were in agreement with those reported by Sperti *et al* (25). However, since such sensitivity, specificity, and accuracy calculations generally depend highly on the underlying prevalence of the disease, one should also consider the underlying prevalence of the diseases, in the comparison of such calculations.

In the use of FDG-PET imaging for the diagnosis of pancreatic tumors, we should remember that the FDG can accumulate in chronic and acute pancreatitis and results in false-positive interpretations on PET imaging. Furthermore, IPMN is sometimes associated with secondary pancreatitis due to disturbance in the run-off of pancreatic juice (29). However, in the present study, the specificity of FDG-PET was 100%, and false-positive PET scans from pancreatitis were not observed.

In addition to the FDG-PET findings, we also examined in the present study the diagnostic utility of conventional modalities including pancreatic duct lavage cytology and/or pancreatic juice cytology and certain imaging parameters, which are known to be associated with a higher likelihood of malignancy. The results of pancreatic duct lavage cytology and/or pancreatic juice cytology also actually helped discriminate benign and malignant tumors in this study. However, cytology frequently results in false-negatives or inconclusive results, and it is of diagnostic value only if cancer is proven. Therefore, it is difficult to compare its usefulness

to that of other modalities. This study also showed the low power of other imaging parameters, apart from mural nodule, such as large/small size of cystic lesion and dilated/non-dilated MPD, in the differentiation of malignant from benign IPMN, which may be partly due to the potential prejudices in selection of the enrolled patients; the enrolled patients might be necessary for surgery. On the other hand, the presence/absence of mural nodule, which has been considered an indicator of malignancy in IPMN, was found to be useful in the differentiation of malignancy in this study (12,13,15-17). The sensitivity, specificity, and accuracy of the presence/absence of mural nodule in the differentiation of malignant IPMN were 93, 80 and 86%, respectively. This diagnostic value of the presence/absence of mural nodule was in agreement with some previous reports (15,16).

In this analysis, the specificity and accuracy of the presence/absence of mural nodule in the differentiation of malignant IPMN were just slightly inferior to those of the FDG-PET findings, and the sensitivity was almost equal, which suggests that we can actually obtain information enough for the differentiation from CT findings alone. However, as shown in Table II and Fig. 4, there were four cases with discrepancy between the presence/absence of mural nodule and histopathological finding (one malignant patient positive on FDG-PET without mural nodule, and three benign patients with mural nodule and negative FDG-PET finding). In all the four cases, the FDG-PET findings with SUVmax cut-off value being 2.5, corresponded perfectly to the histopathological findings. Considering such clinical significance in the FDG-PET, the FDG-PET examination was found significant in combination with CT. Reflecting the result of this study, patients with positive FDG-PET finding despite negative CT findings should be considered as potentially malignant, and be recommended undergoing surgery. On the other hand, now, we cannot exclude PET-negative patients with suspicious malignant CT finding from surgical indication. However, in future, by collecting histopathological information of such patients, some of such patients may be expected to be followed-up without surgical resection.

In addition to the surgically-resected IPMN patients, IPMN patients without surgical resection were investigated. In general, since most IPMNs are generally slow-growing tumors, it is not determined that IPMNs which have been unchanged for a certain period without histopathological confirmation of the resected specimens are considered to be benign (30). For this reason, patients without histopathological confirmation of the resected specimens were excluded from the present study, and only patients with IPMN which had been histopathologically confirmed in resected specimens were included in the present study. However, in the patients without surgical resection, the tumor with the SUVmax <2.5 has been unchanged during the follow-up period, and the tumor with the SUVmax ≥2.5 had grown, which suggests association of tumor progression with the FDG-PET findings. Considering the association, the utility of the FDG-PET in the differentiation of benign and malignant IPMN is suggested to be validated in patients without surgical resection.

In summary, FDG-PET is a useful imaging technique for the diagnosis of malignant IPMN of the pancreas when used with SUVmax cut-off level of 2.5, with specificity, sensitivity and accuracy of 93, 100 and 96%, respectively. We recommend the use of FDG-PET in combination with CT for the diagnosis of malignant IPMN of the pancreas.

References

1. Ohashi K, Murakami Y and Murayama M: Four cases of mucus secreting pancreatic cancer. Prog Dig Endosc 20: 348-351, 19982.
2. Sugiyama M and Atomi Y: Intraductal papillary mucinous tumors of the pancreas: imaging studies and treatment strategies. Ann Surg 228: 685-691, 1998.
3. Sohn TA, Yeo CJ, Cameron JL, Iacobuzio-Donahue CA, Hruban RH and Lillemoe KD: Intraductal papillary mucinous neoplasms of the pancreas: an increasingly recognized clinicopathologic entity. Ann Surg 234: 313-321, 2001.
4. Suzuki Y, Atomi Y, Sugiyama M, *et al*: Japanese multi-institutional study of intraductal papillary mucinous tumor and mucinous cystic tumor. Cystic neoplasm of the pancreas: a Japanese multiinstitutional study of intraductal papillary mucinous tumor and mucinous cystic tumor. Pancreas 28: 241-246, 2004.
5. Yamaguchi K, Ogawa Y, Chijiiwa K and Tanaka M: Mucin-hypersecreting tumors of the pancreas: assessing the grade of malignancy preoperatively. Am J Surg 171: 427-431, 1996.
6. Kloppel G, Solcia E, Longnecker DS, Capella C and Sobin LH: Histological typing of tumours of the exocrine pancreas. In: World Health Organization. International Histological Classification of Tumors. 2nd edition. Springer, Berlin, pp11-20, 1996.
7. Yamao K, Ohashi K, Nakamura T, *et al*: The prognosis of intraductal papillary mucinous tumors of the pancreas. Hepatogastroenterology 47: 1129-1134, 2000.
8. Salvia R, Fernández-del Castillo C, Bassi C, *et al*: Main-duct intraductal papillary mucinous neoplasms of the pancreas: clinical predictors of malignancy and long-term survival following resection. Ann Surg 239: 678-685, 2004.
9. Cellier C, Cuillerier E, Palazzo L, *et al*: Intraductal papillary and mucinous tumors of the pancreas: accuracy of preoperative computed tomography, endoscopic retrograde pancreatography and endoscopic ultrasonography, and long-term outcome in a large surgical series. Gastrointest Endosc 47: 42-49, 1998.
10. Bernard P, Scoazec JY, Joubert M, Kahn X, Le Borgne J, Berger F and Partensky C: Intraductal papillary-mucinous tumors of the pancreas: predictive criteria of malignancy according to pathological examination of 53 cases. Arch Surg 137: 1274-1278, 2002.
11. Sugiyama M, Izumisato Y, Abe N, Masaki T, Mori T and Atomi Y: Predictive factors for malignancy in intraductal papillary-mucinous tumours of the pancreas. Br J Surg 90: 1244-1249, 2003.
12. Baba T, Yamaguchi T, Ishihara T, *et al*: Distinguishing benign from malignant intraductal papillary mucinous tumors of the pancreas by imaging techniques. Pancreas 29: 212-217, 2004.
13. Itoh T, Hirooka Y, Itoh A, *et al*: Usefulness of contrast-enhanced transabdominal ultrasonography in the diagnosis of intraductal papillary mucinous tumors of the pancreas. Am J Gastroenterol 100: 144-152, 2005.
14. Jang JY, Kim SW, Ahn YJ, *et al*: Multicenter analysis of clinicopathologic features of intraductal papillary mucinous tumor of the pancreas: is it possible to predict the malignancy before surgery? Ann Surg Oncol 12: 124-132, 2005.
15. Chiu SS, Lim JH, Lee WJ, *et al*: Intraductal papillary mucinous tumour of the pancreas: differentiation of malignancy and benignancy by CT. Clin Radiol 61: 776-783, 2006.
16. Takeshita K, Kutomi K, Takada K, *et al*: Differential diagnosis of benign or malignant intraductal papillary mucinous neoplasm of the pancreas by multidetector row helical computed tomography: evaluation of predictive factors by logistic regression analysis. J Comput Assist Tomogr 32: 191-197, 2008.
17. Nakamoto Y, Higashi T, Sakahara H, *et al*: Delayed (18)F-fluoro-2-deoxy-D-glucose positron emission tomography scan for differentiation between malignant and benign lesions in the pancreas. Cancer 89: 2547-2554, 2000.
18. Pakzad F, Groves AM and Ell PJ: The role of positron emission tomography in the management of pancreatic cancer. Semin Nucl Med 36: 248-256, 2006.

19. Chen YK, Su CT, Chi KH, Cheng RH, Wang SC and Hsu CH: Utility of 18F-FDG PET/CT uptake patterns in Waldeyer's ring for differentiating benign from malignant lesions in lateral pharyngeal recess of nasopharynx. J Nucl Med 48: 8-14, 2007.
20. Fletcher JW, Kymes SM, Gould M, *et al*: VA SNAP Cooperative Studies Group. A comparison of the diagnostic accuracy of 18F-FDG PET and CT in the characterization of solitary pulmonary nodules. J Nucl Med 49: 179-185, 2008.
21. Sperti C, Pasquali C, Chierichetti F, Liessi G, Ferlin G and Pedrazzoli S: Value of 18-fluorodeoxyglucose positron emission tomography in the management of patients with cystic tumors of the pancreas. Ann Surg 234: 675-680, 2001.
22. Yoshioka M, Sato T, Furuya T, *et al*: Positron emission tomography with 2-deoxy-2-[(18)F] fluoro-d-glucose for diagnosis of intraductal papillary mucinous tumor of the pancreas with parenchymal invasion. J Gastroenterol 38: 1189-1193, 2003.
23. Sperti C, Pasquali C, Decet G, Chierichetti F, Liessi G and Pedrazzoli S: F-18-fluorodeoxyglucose positron emission tomography in differentiating malignant from benign pancreatic cysts: a prospective study. J Gastrointest Surg 9: 22-28, 2005.
24. Mansour JC, Schwartz L, Pandit-Taskar N, *et al*: The utility of F-18 fluorodeoxyglucose whole body PET imaging for determining malignancy in cystic lesions of the pancreas. J Gastrointest Surg 10: 1354-1360, 2006.
25. Sperti C, Bissoli S, Pasquali C, Frison L, Liessi G, Chierichetti F and Pedrazzoli S: 18-fluorodeoxyglucose positron emission tomography enhances computed tomography diagnosis of malignant intraductal papillary mucinous neoplasms of the pancreas. Ann Surg 246: 932-937, 2007.
26. Paul AK, Tatsumi M, Higuchi I, Fukunaga H, Yasuda T and Nishimura T: Gamma camera coincidence imaging with [^{18}F] fluorodeoxyglucose in the pretreatment evaluation of patients with oesophageal cancer. Nucl Med Commun 24: 963-970, 2003.
27. Tatsumi M, Yutani K, Watanabe Y, *et al*: Feasibility of fluorodeoxyglucose dual-head gamma camera coincidence imaging in the evaluation of lung cancer: comparison with FDG PET. J Nucl Med 40: 566-573, 1999.
28. Fukunaga H, Sekimoto M, Ikeda M, *et al*: Fusion image of positron emission tomography and computed tomography for the diagnosis of local recurrence of rectal cancer. Ann Surg Oncol 12: 561-569, 2005.
29. Goh BK, Tan YM, Cheow PC, Chung YF, Chow PK, Wong WK and Ooi LL: Cystic neoplasms of the pancreas with mucin-production. Eur J Surg Oncol 31: 282-287, 2005.
30. Tanaka M: Intraductal papillary mucinous neoplasm of the pancreas: diagnosis and treatment. Pancreas 28: 282-288, 2004.

Published OnlineFirst June 8, 2010; DOI:10.1158/0008-5472.CAN-09-4313

Microenvironment and Immunology

Cancer Research

Increased Immunogenicity of Tumor-Associated Antigen, Mucin 1, Engineered to Express α-Gal Epitopes: A Novel Approach to Immunotherapy in Pancreatic Cancer

Takashi Deguchi[1], Masahiro Tanemura[1], Eiji Miyoshi[2], Hiroaki Nagano[1], Tomohiko Machida[1], Yoshiaki Ohmura[1], Shogo Kobayashi[1], Shigeru Marubashi[1], Hidetoshi Eguchi[1], Yutaka Takeda[1], Toshinori Ito[3], Masaki Mori[1], Yuichiro Doki[1], and Yoshiki Sawa[4]

Abstract

Mucin 1 (MUC1), a bound mucin glycoprotein, is overexpressed and aberrantly glycosylated in >80% of human ductal pancreatic carcinoma. Evidence suggests that MUC1 can be used as a tumor marker and is a potential target for immunotherapy of pancreatic cancer. However, vaccination with MUC1 peptides fails to stimulate the immune response against cancer cells because immunity toward tumor-associated antigens (TAA), including MUC1, in cancer patients is relatively weak, and the presentation of these TAAs to the immune system is poor due to their low immunogenicity. We investigated whether vaccination with immunogenetically enhanced MUC1 (by expressing α-gal epitopes; Galα1-3Galβ1-4GlcNAc-R) can elicit effective antibody production for MUC1 itself as well as certain TAAs derived from pancreatic cancer cells and induced tumor-specific T-cell responses. We also used α1,3galactosyltransferase (α1,3GT) knockout mice that were preimmunized with pig kidney and transplanted with B16F10 melanoma cells transfected with MUC1 expression vector. Vaccination of these mice with α-gal MUC1 resulted in marked inhibition of tumor growth and significant improvement of overall survival time compared with mice vaccinated with MUC1 alone ($P = 0.003$). Furthermore, vaccination with pancreatic cancer cells expressing α-gal epitopes induced immune responses against not only differentiated cancer cells but also cancer stem cells. The results suggested that vaccination using cells engineered to express α-gal epitopes is a novel strategy for treatment of pancreatic cancer. *Cancer Res; 70(13); 5259–69. ©2010 AACR.*

Introduction

Pancreatic cancer is the fourth most common cause of death from cancer in men and women, with 5-year survival for all stages of disease of <5% (1–3). Surgical resection remains the only potentially curative intervention but is contraindicated in most patients because the disease is diagnosed at an advanced stage. Potential treatments of pancreatic cancer include immunotherapy, gene therapy, and antiangiogenic agents.

Immunotherapy is an innovative approach that uses techniques such as vaccination to activate the patient's immune system tumor-associated antigens (TAA) expressed in pancreatic cancer cells. Mucin 1 (MUC1) is one of the most considerable targets for vaccine immunotherapy (4, 5). It is a type I transmembrane protein composed of a heavily glycosylated extracellular domain containing a variable number of tandem repeats, a transmembrane domain, and a cytoplasmic domain (6–9). MUC1 is normally expressed on the apical surface of ductal and glandular epithelial cells. In benign cells of breast, prostate, ovarian, and pancreas, MUC1 is heavily glycosylated, limited to the apical side of the glands, and minimally expressed. Transformation of these cells into malignant cells is associated with the overexpression of MUC1, loss of MUC1 expression polarity, and dysregulation of *O*-glycans of MUC1 (6–8). Consequent to aberrant expression of a series of glycosyltransferases, the tumor-associated MUC1 carries a preponderance of shorter glycans (6–9). The ultimate result of these changes is the exposure of normally cryptic portions of the core protein structure, consisting of the tandem repeat array, which is the most immunogenic part of MUC1, toward the effector cells of the patient's immune system; therefore, MUC1 is considered a potential target for vaccine therapies.

In fact, MUC1 vaccines were tested in several clinical trials (10–13). However, they have not been as successful as hoped, in part due to the immune evasion tactics applied by tumor

Authors' Affiliations: Departments of [1]Surgery, Gastroenterological Surgery, [2]Molecular Biochemistry and Clinical Investigation, [3]Complementary & Alternative Medicine, and [4]Surgery, Cardiovascular Surgery, Osaka University Graduate School of Medicine, 2-2 Yamadaoka, Suita, Osaka, Japan

Note: Supplementary data for this article are available at Cancer Research Online (http://cancerres.aacrjournals.org/).

Corresponding Author: Masahiro Tanemura, Graduate School of Medicine, Osaka University, 2-2 Yamadaoka E-2, Suita, Osaka 565-0871, Japan. Phone: 81-6-6879-3251; Fax: 81-6-6879-3259; E-mail: mtanemura@gesurg.med.osaka-u.ac.jp.

doi: 10.1158/0008-5472.CAN-09-4313

Published OnlineFirst June 8, 2010; DOI:10.1158/0008-5472.CAN-09-4313

cells to escape immunorecognition (14, 15). A prerequisite for the induction of an effective antitumor immune response by MUC1 vaccine is the effective uptake of this molecule by professional antigen-presenting cells (APC). Thus, processing of the internalized MUC1 in the vaccine, and presentation of antigenic MUC1 peptides on APCs in association with MHC class I and class II molecules, could activate antitumor cytotoxic T cells and helper T cells. However, MUC1 proteins on pancreatic cancer cells do not express markers that contain modification of MUC1 to be recognized by APCs. To increase the immunogenicity of MUC1 to APCs, IgG bound to MUC1 could be a suitable strategy. In this study, we hypothesized that IgG-mediated targeting of MUC1 could enhance presentation to APC by exploiting the natural anti-Gal in humans.

Anti-Gal is an IgG antibody (Ab) that is present in large amounts in normal subjects and patients with malignancies, comprising ~1% of serum-circulating IgG (16–18). Anti-Gal Ab specifically interacts with α-gal epitopes on cell surface glycolipids and glycoproteins, and it is produced throughout life due to antigenic stimulation by bacteria of the gastrointestinal flora (19). Once anti-Gal binds to α-gal epitopes on the cell, its Fc portion readily binds to FcγR III on dendritic cells and macrophages. This interaction induces effective phagocytosis of the anti-Gal–opsonized cells by APC (20–22). The α-gal epitopes are absent in humans, but are abundantly synthesized on glycolipids and glycoproteins by the glycosyltransferase enzyme, α1,3galactosyltransferase (α1,3GT) within the Golgi apparatus of cells of nonprimate mammals, prosimians, and in New World monkeys (23). In contrast, humans, apes, and Old World monkeys lack α-gal epitopes; instead, they produce the natural anti-Gal Ab in very large amounts (24, 25). Anti-Gal Ab is an Ab that can be very active *in vivo*, as inferred from studies in xenotransplantation (26, 27). The *in vivo* binding of anti-Gal Ab to α-gal epitopes on transplanted pig heart or kidney is the main cause of hyperacute rejection of such grafts in humans and in Old World monkeys. Similarly, we hypothesized that MUC1 vaccine processed to express α-gal epitopes (MUC1 has five potential sites of *N*-glycans that are targets for α1,3GT) can bind the natural anti-Gal IgG Ab *in situ* at the vaccination site. Such interaction would enhance recognition by APCs, resulting in more effective vaccination.

In the present study, we investigated the effects of vaccination with α-gal MUC1 on pancreatic cancer cells and examined its usefulness in the induction of tumor-specific T-cell responses, *in vivo* prevention of tumor growth, and prolongation of survival of α-gal MUC1 vaccine recipients. A rare population of cells with stem cell properties called cancer stem cells was identified recently. In 2007, Li and colleagues (28) reported that $CD44^+CD24^+$ epithelial-specific antigen $(ESA)^+$ pancreatic cancer cells showed stem cell properties. It is necessary to develop an effective therapy for cancer stem cells to eradicate cancer cells; however, cancer stem cells are highly resistant to adjuvant therapy including chemotherapy. We hypothesized that biosynthesis of α-gal epitopes on the carbohydrate of cancer stem cell markers expressed on pancreatic cancer stem cells could effectively induce Ab production against these stem cells. We also investigated the immune response induced by vaccines expressing α-gal epitopes against both differentiated pancreatic cancer cells and pancreatic cancer stem cells.

Materials and Methods

Flow cytometry

To evaluate the expression of α-gal epitopes on the cell surface of α-gal PANC1 cells, flow cytometric analysis was performed. Parental PANC1 and α1,3GT transfectants were incubated with 20 μg/mL biotinylated GS1B4 lection (Vector Laboratories), which specifically binds to α-gal epitopes or the monoclonal anti-Gal Ab M86 (29–35). Details of the procedure were previously described (26–30).

To examine the endogenous expression of MUC1 protein, cells were primarily stained with anti-MUC1 monoclonal Ab (mAb; clone VU4H5, Santa Cruz Biotechnology), and subsequently, cells were incubated with FITC-conjugated anti-mouse immunoglobulins as a secondary Ab (DAKO). Stained cells were washed, fixed, and then analyzed by a flow cytometer.

To evaluate the expression of CD44, CD24, and ESA, which are stem cell markers of pancreatic cancer cells on parental PANC1, parental PANC1 cells were stained with either FITC-conjugated antihuman CD24 mAb, phycoerythrin-conjugated antihuman CD44 mAb or FITC-conjugated antihuman ESA mAb, respectively, as previously described (BD Biosciences; ref. 36). To investigate Ab production against pancreatic cancer stem cells, isolated stem cells from PANC1 cells were stained with sera from vaccinated knockout (KO) mice. Cancer stem cells expressing both CD44 and CD24 were positively isolated by streptavidin-coated Dynalbeads M-280. The magnetic beads were incubated with either biotinylated antihuman CD24 mAb or antihuman CD44 mAb, respectively (Ancell Corp.). Subsequently, 10×10^6 cells of parental PANC1 cells were incubated with anti-CD44 mAb-coated beads in 1% bovine serum albumin (BSA)/PBS for 2 hours at 4°C, and the CD44-positive cells were positively isolated by DynaMag (Invitrogen). The isolated cells were then incubated with anti-CD24 mAb-coated beads in a similar manner. Subsequently, CD44– and CD24–double-positive cells were isolated by DynaMag (Invitrogen). The isolated $CD44^+CD24^+$ pancreatic cancer cells were incubated with sera from KO mice that had been vaccinated with either parental PANC1 or α-gal PANC1 cells. Subsequently, these cells were stained with FITC-conjugated anti-mouse IgG1 (Bethyl Laboratories, Inc.) as a secondary Ab to detect Abs that interact with the pancreatic cancer stem cells. Moreover, PANC1 cells that did not bind with either anti-CD44 mAb– or anti-CD24 mAb–coated beads were combined and incubated with KO mice sera to assess reactivity with differentiated pancreatic cancer cells other than $CD44^+CD24^+$ cells.

Tumor cell vaccination

α1,3GT KO mice were immunized by pig kidney fragments, and the presence of anti-Gal in their serum was confirmed by ELISA as described above. Subsequently, the mice were vaccinated i.p. thrice at 1-week intervals with 1×10^6

Published OnlineFirst June 8, 2010; DOI:10.1158/0008-5472.CAN-09-4313

50 Gy–irradiated parental PANC1 or α-gal PANC1 cells. One week after vaccination, the mice were assessed for the immune response elicited by tumor cell vaccination as described below.

Enzyme-linked immunospot analysis

The enzyme-linked immunospot (ELISPOT) assay was used to measure the expansion of anti-MUC1–secreting B cells or MUC1-specific T cells, respectively (30, 37, 38). ELISPOT wells (MultiScreen 96-well Filtration Plate, Millipore) were coated with either MUC1-BSA (10 μg/mL) or BSA (5 μg/mL) for 20 hours at 4°C, then blocked overnight with RPMI containing 0.4% BSA and 50 μmol/L of 2-mercaptoethanol. Splenocytes prepared from mice that had been vaccinated with α-gal PANC1 cells or parental PANC1 cells were plated in the wells at a concentration of 1×10^6 cells per well, and the plates were incubated for 24 hours at 37°C. Subsequently, the wells were washed, incubated with horseradish peroxidase (HRP)–conjugated goat antimouse immunoglobulin (Bethyl Laboratories, Inc.), and the spots representing Abs secreted from individual plasma cells were identified with diaminobenzidine (DAB, Sigma-Aldrich). The number of anti-MUC1 producing plasma cells in each well was determined by subtracting the background number of spots in wells containing BSA as solid-phase antigen from the number of spots in the corresponding wells with MUC1-BSA.

To identify MUC1-specific T cells in the vaccinated KO mice, the secretion of IFN-γ from the activated T cells was measured by ELISPOT assay. ELISPOT plates were coated with anti–IFN-γ mAb (clone AN18, Mabtech). Splenocytes were incubated in the coated ELISPOT wells (1×10^6 cells/well) in the presence or absence of 100 μg/mL MUC1 peptide. Furthermore, to investigate whether the reactivity of MUC1-specific T cells was mediated through MHC class I, splenocytes were incubated in the wells in the presence of both 100 mg/mL MUC1 peptide and mouse antimouse H-2D^b mAb as anti-MHC class I–blocking Ab (BD Biosciences) at a dilution of 1:50. After 24 hours of incubation at 37°C, the wells were washed and then stained with biotinylated anti–IFN-γ mAb (clone R4-6A2, Mabtech) for 1 hour at room temperature. Subsequently, the wells were washed, incubated with HRP-conjugated streptavidin (DAKO), and the spots representing activated T cells were developed with DAB. The numbers of developed spots in ELISPOT assays were counted by the ChemiDoc XRS image analyzer (Bio-Rad Laboratories) using Quantity one software (Bio-Rad).

***In vivo* studies of tumor cell vaccine in an experimental animal model**

The efficacy of tumor vaccines expressing α-gal epitopes cannot be studied in a regular experimental animal model because normal wild-type mouse cells and the majority of mouse tumor cell lines, including mouse pancreatic cancer, express α-gal epitopes. Therefore, B16F10 melanoma cells (American Type Culture Collection) from C57BL/6 mice were used in the present study because they lack α-gal epitopes caused by inactivation of the *α1,3GT* gene (30). First, B16F10 cells were transfected with the full-length *MUC1* gene (5, 39), using Lipofectamine, and a stable B16F10 transfectant expressing MUC1 protein was established (designated MUC1-B16F10). High anti-Gal KO mice were generated by immunization with pig kidney fragments then vaccinated with parental PANC1 or α-gal PANC1 cells after irradiation. One week later, all mice were challenged with s.c. injection with 0.5×10^6 live MUC1-B16F10 cells. Subsequently, mice were examined serially for both tumor growth and survival. The production of anti-MUC1 Abs and Abs toward other tumor antigens was examined by Western blot analysis, using *α1,3GT* KO mice sera. Subsequently, 3 μg of cellular proteins extracted from PANC1 were loaded to 6% SDS-PAGE and transferred onto a polyvinylidene difluoride membrane. After blocking with PBS containing 3% BSA, the blot was incubated for 20 hours at 4°C with *α1,3GT* KO mice serum obtained from either nonimmunized, high anti-Gal, parental PANC1–vaccinated, or α-gal PANC1–vaccinated KO mice at 1:20 dilution, respectively. After washing, the blot was incubated with HRP-conjugated anti-mouse IgG (Bethyl Laboratories) as the secondary Ab and developed using the enhanced chemiluminescence detection system.

Details of the mice used in these experiments, cell lines, gene construct, methods used to establish stable pancreatic cancer cells expressing α-gal epitopes, Western blot analysis and immunoprecipitation, *in vitro* stimulation of lymphocytes, ELISA, and statistical analysis are presented as Supplementary Material in the electronic version of the journal.

Results

Generation of stable PANC1 transfectant expressing α-gal epitopes

No expression of α-gal epitopes was observed in parental PANC1 cells, whereas high expression levels of α-gal epitopes were observed on the cell surface of α1,3GT transfectants (Fig. 1A). Similar levels of MUC1 expression were observed in parental PANC1 and α-gal PANC1 cells on both flow cytometry and Western blot analyses (Fig. 1B). Immunoprecipitation with anti-Gal Ab showed a strong band at 150 kDa, which was consistent with MUC1 (Fig. 1B).

Vaccination with α-gal PANC1 elicits the production of anti-Gal and anti-MUC1 Abs

The anti-Gal Ab, as a natural Ab, was negative in nonimmunized *α1,3GT* KO mice. Repeated immunizations (four times) with pig kidney fragments resulted in the appearance of anti-Gal Ab, with the titer of anti-Gal IgG being similar to that observed in a large proportion of human sera (Fig. 1C and D; refs. 23, 24). As shown in Fig. 1C, vaccination with α-gal PANC1 resulted in 8-fold increase in production of anti-Gal IgG compared with high anti-Gal KO mice generated by pig kidney immunization. In contrast, no significant increase in the titer of anti-Gal IgG was detected when anti-Gal KO mice were vaccinated with parental PANC1 cells (Fig. 1D). A similar difference in anti-MUC1 IgG response was observed in mice vaccinated with either α-gal PANC1 or parental PANC1 cells. Three vaccinations

Published OnlineFirst June 8, 2010; DOI:10.1158/0008-5472.CAN-09-4313

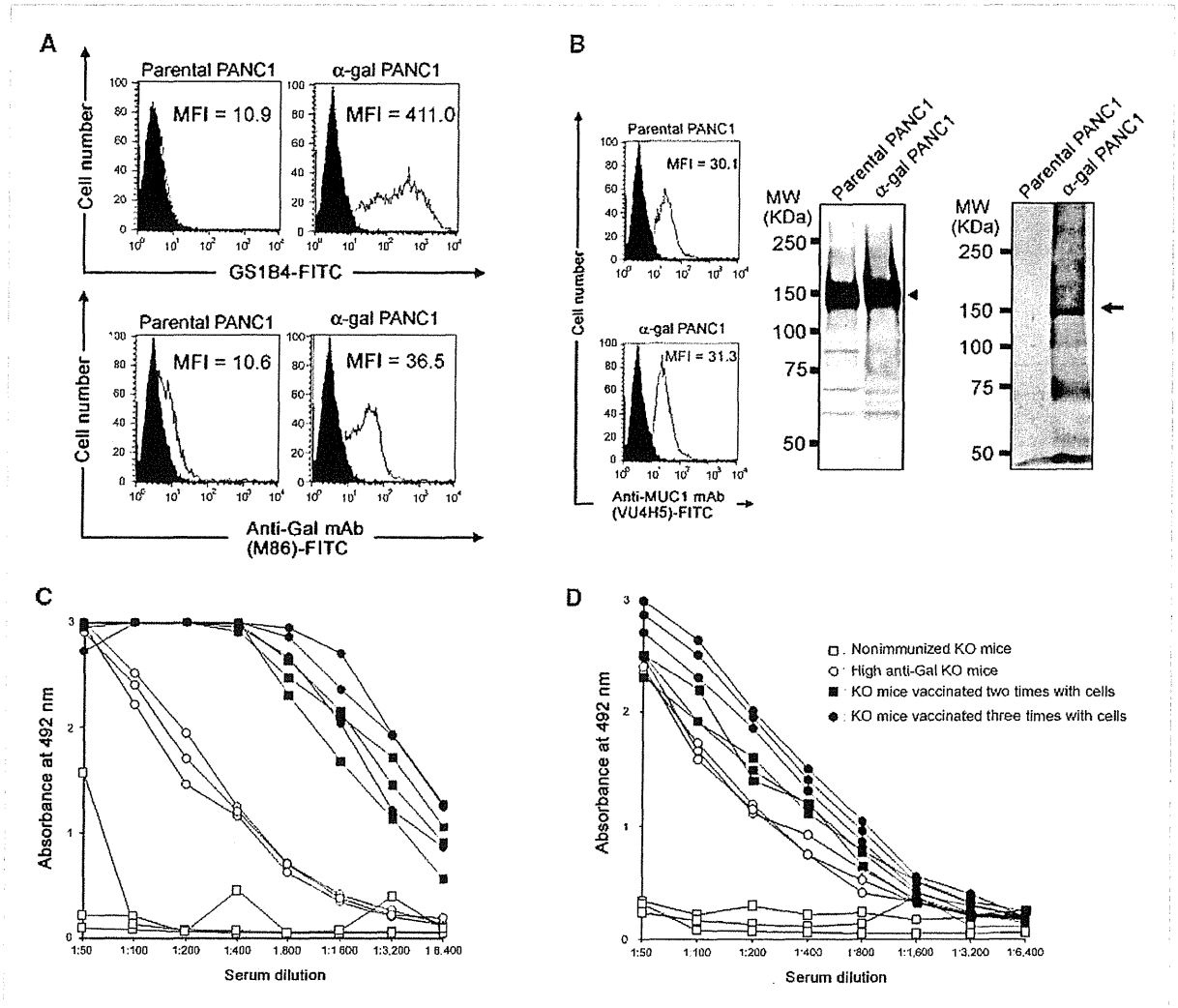

Figure 1. Expression levels of α-gal epitopes on MUC1 proteins in α-gal PANC1 (top) and anti–Gal IgG production in vaccinated KO mice (bottom). A, the expression levels of α-gal epitopes in either parental PANC1 or α-gal PANC1. Closed histogram, unstained cells; open histogram, stained cells with either GS1B4 lection or M86 mAb. MFI, mean fluorescence intensity. B, the expression levels of endogenous MUC1 protein and α-gal epitopes on MUC1 protein were examined. Left, flow cytometry; closed histogram, unstained cells; open histogram, stained cells with anti-MUC1 mAb. Middle, Western blotting analysis; arrowhead, MUC1 protein band. Right, immunoprecipitation assay; arrow, the band of α-gal epitopes on MUC1 protein; MW, molecular weight. C, anti-Gal IgG production in sera from α-gal PANC1–vaccinated KO mice. D, anti-Gal IgG production in sera from parental PANC1–vaccinated KO mice. Representative data of five experiments with similar results. ELISA results represent three data sets from five mice per group.

with 1×10^6 of α-gal PANC1 elicited a strong anti-MUC1 IgG response, whereas vaccination with parental PANC1 cells did not elicit such an Ab response (Fig. 2A and B). Approximately 8- to 16-fold increase in anti-MUC1 IgG production was elicited by α-gal PANC1 vaccination compared with parental PANC1 vaccination (Fig. 2A and B). Analysis of anti-MUC1 isotypes in sera from KO mice vaccinated with α-gal PANC1 cells showed large production of anti-MUC1 IgG, a small amount of anti-MUC1 IgM, but no IgA isotype (Supplementary Fig. S1A). The isotypes of immunoglobulin reactivities in the sera from parental PANC1–vaccinated KO mice also showed a similar pattern of anti-MUC1 isotypes to that of sera from α-gal PANC1–vaccinated mice (Supplementary Fig. S1B).

Analysis of IgG subclasses of anti-MUC1 IgG response in α-gal PANC1–vaccinated mice showed relatively large amounts of IgG1 (Fig. 2C), IgG2b, and IgG3 subclasses of anti-MUC1 IgG, but no IgG2a subclass of this Ab (Fig. 2C). On the other hand, similar analysis of IgG subclasses of this Ab response in parental PANC1–vaccinated mice showed small amounts of IgG1 production, but no IgG2a, IgG2b, and IgG3 subclasses (Fig. 2D).

Published OnlineFirst June 8, 2010; DOI:10.1158/0008-5472.CAN-09-4313

Vaccination with α-gal PANC1 results in the expansion of systemic B- and T-cell response to MUC1

The marked increase in anti-MUC1 IgG titers in mice vaccinated with α-gal PANC1 was associated with expansion of the B-cell clone with anti-MUC1. As shown in Fig. 3A, the expansion of anti-MUC1–secreting B cells was detected *in vitro* by ELISPOT assay with MUC1-BSA as the solid-phase antigen. Splenocytes obtained from high anti-Gal KO mice without PANC1 vaccination displayed no dots in ELISPOT wells (data not shown). Parental PANC1–vaccinated KO mice had 319.5 ± 18.9 spots per 1×10^6 splenocytes. However, α-gal PANC1–vaccinated KO mice displayed 553.6 ± 66.7 spots per 1×10^6 splenocytes, and the proportion of anti-MUC1 B cells was significantly increased ($P < 0.0001$; Fig. 3A).

The priming of T cells, which specifically react with MUC1 peptide, was also determined by ELISPOT assay, by measuring IFN-γ secretion following the *in vitro* activation of T cells in the presence of MUC1 peptide. In parental PANC1–vaccinated KO mice, 211 ± 33.4 and 153.2 ± 15.2 spots per 1×10^6 splenocytes were detected in the presence or absence of MUC1 peptide, respectively, and no significant increase in the number of spots was observed (Fig. 3B). In contrast, α-gal PANC1–vaccinated KO mice displayed 1,237.5 ± 283.1 spots per 1×10^6 splenocytes in the presence of MUC1 peptides and 313.8 ± 48.9 spots in the absence of MUC1 peptides.

In the blocking assay, anti-MHC class I mAb completely blocked the elicited increase in the number of spots observed in α-gal PANC1–vaccinated KO mice. Splenocytes treated with anti-MHC class I mAb displayed 316 ± 70.4 spots, and this number of spots was comparable with that in the absence of MUC1 peptides (Fig. 3B). In parental PANC1–vaccinated KO mice, no significant blocking effects for anti-MHC class I mAb were observed (169.5 ± 15.2 spots/1×10^6 splenocytes, Fig. 3B). Taken together, KO mice vaccinated with α-gal PANC1 displayed a significant expansion of both B- and T-cell responses to MUC1 (Fig. 3A and B). Furthermore, such elicited T-cell responses against MUC1 peptide were induced through MHC class I molecule.

Immune responses of α-gal PANC1–vaccinated α1,3GT KO mice are significantly stronger and more specific against PANC1 cells and MUC1 peptide

As shown in Fig. 3C and D, proliferation of lymphocytes significantly induced in the presence of parental PANC1, α-gal PANC1, or MUC1 peptide was likely to result from specific immune response to vaccination with either parental PANC1 or α-gal PANC1 because lymphocytes obtained from

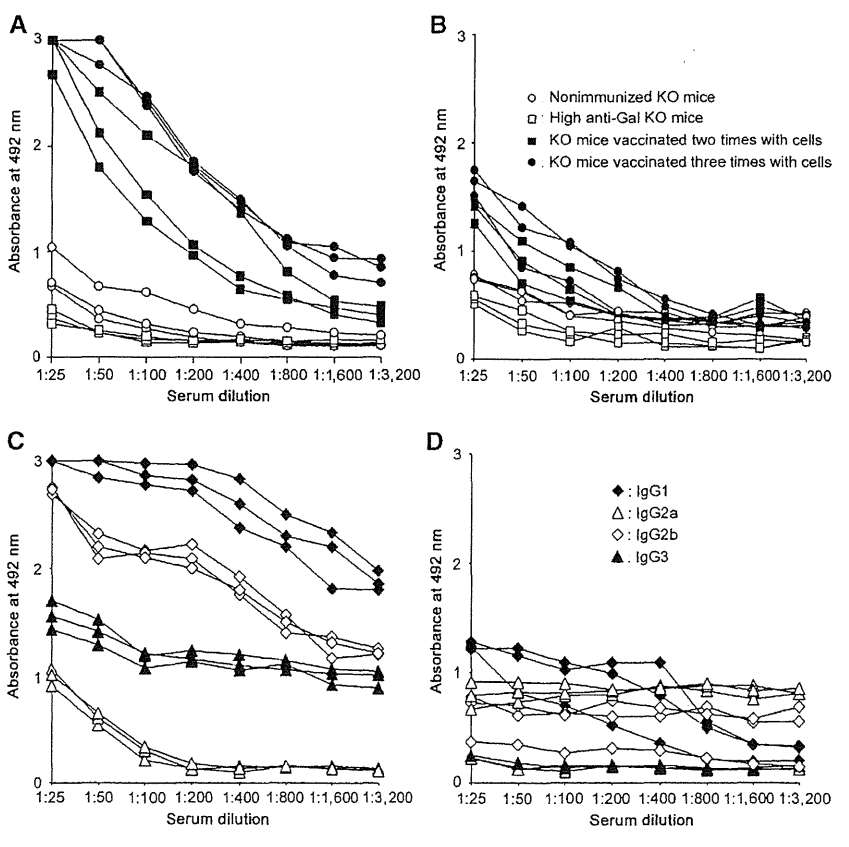

Figure 2. Anti-MUC1 IgG production and subclass of anti-MUC1 IgG assessed by ELISA. A, anti-MUC1 IgG production in KO mice vaccinated by α-gal PANC1. B, anti-MUC1 IgG production in KO mice vaccinated by parental PANC1. C, subclass of anti-MUC1 IgG in KO mice vaccinated by α-gal PANC1. D, subclass of anti-MUC1 IgG in KO mice vaccinated by parental PANC1. ELISA results represent three data sets from five mice per group.

Published OnlineFirst June 8, 2010; DOI:10.1158/0008-5472.CAN-09-4313

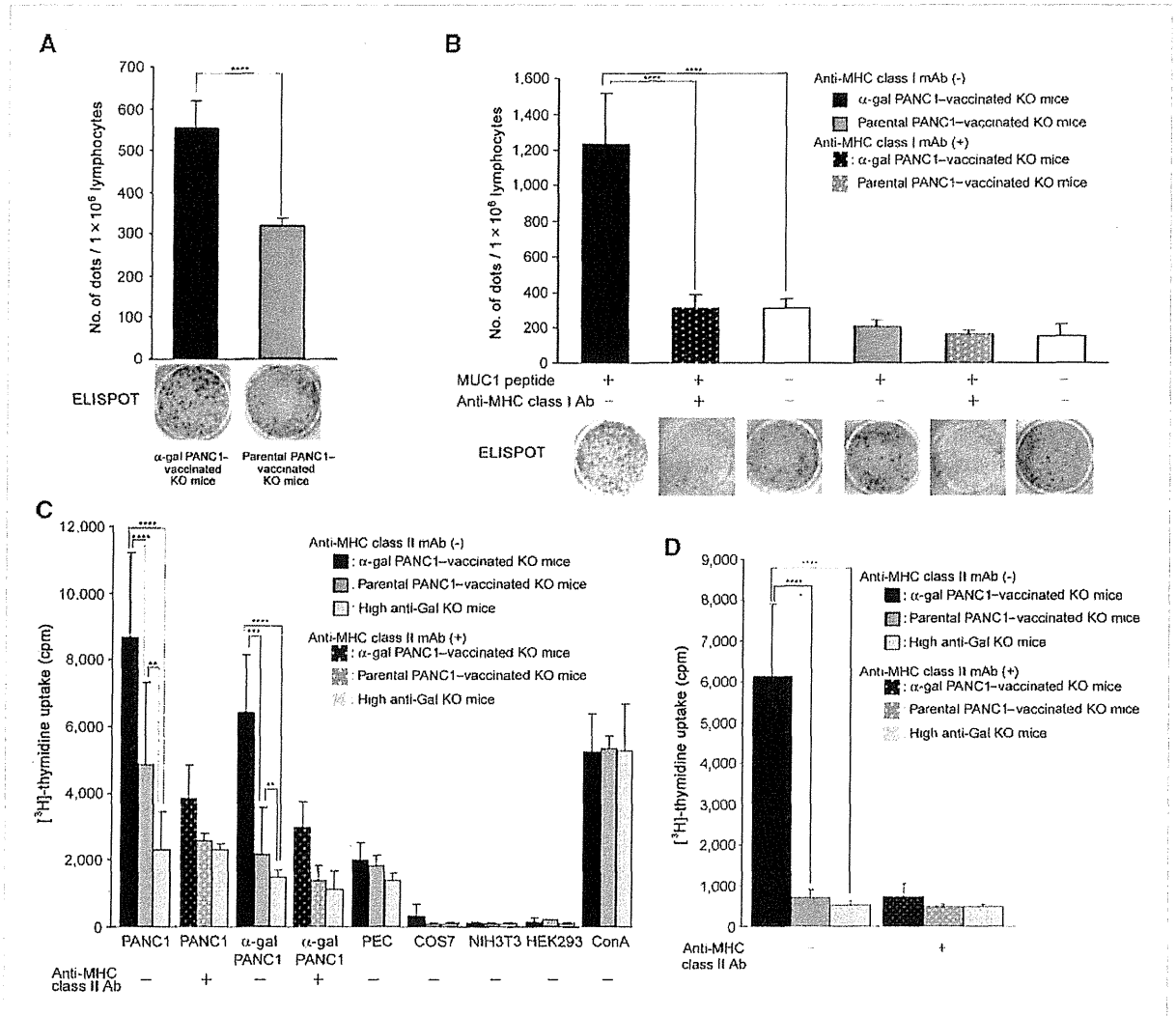

Figure 3. Expansion of B and T cells in response to cell vaccination. A, ELISPOT assay for anti-MUC1 Ab–producing B cells with lymphocytes from α-gal PANC1–vaccinated KO mice or parental PANC1–vaccinated KO mice. B, ELISPOT assay for *in vitro* activated T cells detected by the secretion of INF-γ with or without anti-MHC class I Ab. C, proliferation assay of spleen lymphocytes from α-gal PANC1– and parental PANC1–vaccinated KO mice with or without anti-MHC class II Ab assessed by MLR. D, proliferation assay of spleen lymphocytes from α-gal PANC1– and parental PANC1–vaccinated KO mice stimulated by MUC1 peptide, with or without anti-MHC class II Ab. Points, mean of five independent experiments; bars, SD. Statistical analyses were performed by the Student's *t* test.

both nonimmunized *α1,3GT* KO mice and *α1,3GT* KO mice bearing high levels of anti-Gal Ab displayed almost no proliferative response when incubated with parental PANC1, α-gal PANC1, or MUC1 peptide. Furthermore, the elicited immune responses expressed by lymphocytes from α-gal PANC1–vaccinated *α1,3GT* KO mice were significantly stronger than those from parental PANC1–vaccinated *α1,3GT* KO mice ($P < 0.001$–0.01). Pig endothelial cells stimulated the proliferation of lymphocytes from both vaccinated KO mice and high anti-Gal KO mice.

Lymphocyte stimulation was also tested with irradiated cells from other species, including monkey COS7 cells, mouse fibroblast NIH3T3 cells, and human HEK293 cells. All types of stimulatory cells failed to induce lymphocyte proliferation. These data indicate that a significant proportion of the stimulatory effect was due to the specific recognition of peptide antigens present in PANC1 cells and MUC1 peptide but absent in mouse, monkey, or human cells. Interestingly, the proliferation induced by α-gal PANC1 cells was slightly lower than that induced by parental PANC1 cells. However, the proliferation rate observed in α-gal PANC1–vaccinated mice was significantly higher than in parental PANC1–vaccinated mice. In all the assays, the lymphocytes were viable and competent

Published OnlineFirst June 8, 2010; DOI:10.1158/0008-5472.CAN-09-4313

because they effectively proliferated as a result of nonspecific stimulation by concanavalin A.

In the blocking assay with anti-MHC class II mAb, specific lymphocyte proliferation elicited by vaccination with α-gal PANC1 was significantly reduced by ~50% (Fig. 3C). Moreover, the specific immune response against MUC1 peptide expressed by lymphocytes from α-gal PANC1–vaccinated KO mice was also markedly suppressed by treatment with anti-MHC class II mAb (Fig. 3D). Taken together, these results indicate that the specific immune responses against PANC1 and MUC1 peptide are mainly induced through MHC class II molecule.

α-gal PANC1 vaccines protect and prolong survival against tumor challenge using MUC1-B16F10 cells

As shown in Fig. 4A, α1,3GT KO mice immunized with pig kidney fragments were vaccinated with 1×10^6 irradiated parental PANC1 or α-gal PANC1 cells. The efficiency of such vaccines was assessed by measuring the ability of irradiated α-gal PANC1 cell vaccines to induce a protective immune response against challenge with live MUC1-expressing B16F10 cells. Before the *in vivo* study, we established the same B16F10 clones that stably expressed MUC1. Although the parental B16F10 cells did not react with anti-MUC1 mAb (VU4H5), *MUC1*-transfected B16F10 cells showed strong reactivity with this mAb (Fig. 4B). The expression level of *MUC1* gene in B16F10 transfectant was similar to that in parental PANC1 cells.

Representative pictures of mice treated with either α-gal PANC1 or parental PANC1 vaccines are shown in Fig. 4C. The tumor size in each mouse treated with α-gal PANC1 vaccines was much smaller than that of mice treated with parental PANC1 vaccines. Approximately 80% of parental PANC1–vaccinated mice died within 20 to 26 days postchallenge, whereas 75% to 80% of mice treated with α-gal PANC1 vaccine were still alive at 30 days after tumor implantation

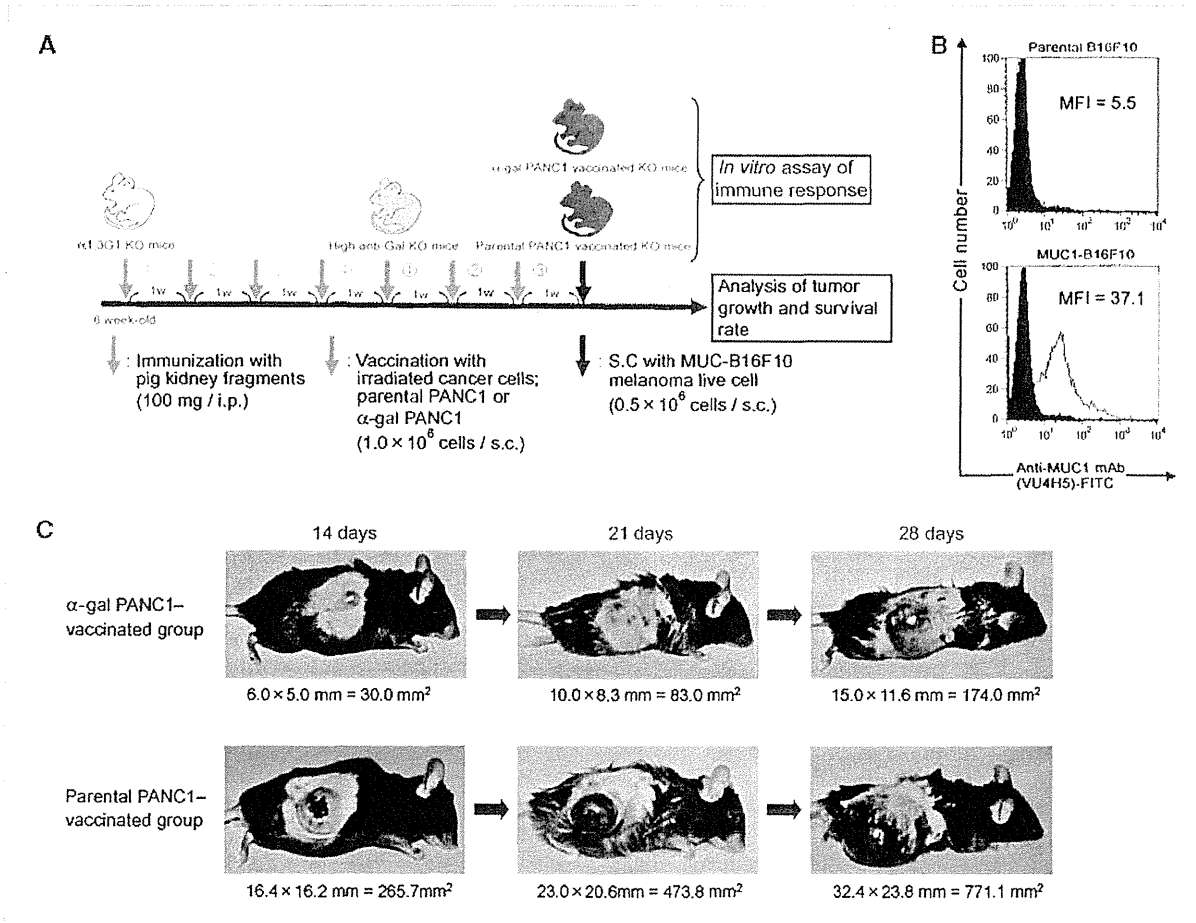

Figure 4. Experimental design for *in vivo* studies and the establishment of MUC1-B16F10. A, schematic illustration of experimental protocol. B, expression levels of MUC1 proteins in parental B16F10 and MUC1-B16F10 transfectant were examined by flow cytometry. Closed histogram, unstained cells; open histogram, stained cells with VU4H5 mAb. C, photographs of the growing tumors in vaccinated KO mice after tumor cell challenge with MUC1-B16F10 cells at days 14, 21, and 28.

Published OnlineFirst June 8, 2010; DOI:10.1158/0008-5472.CAN-09-4313

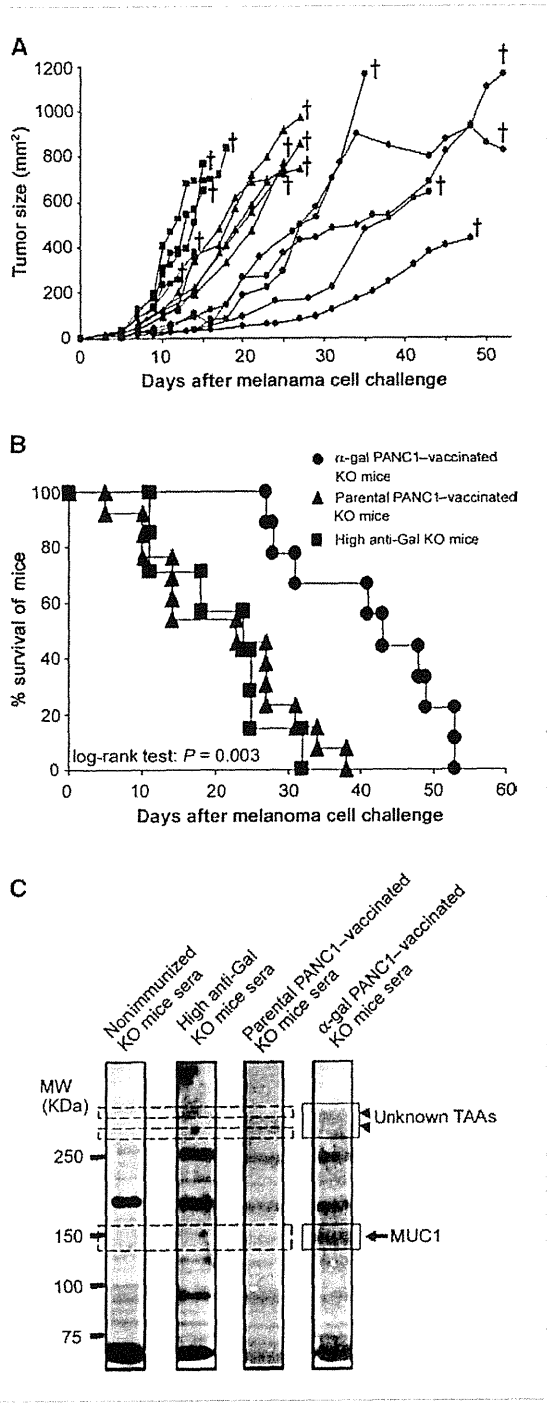

Figure 5. *In vivo* prevention of tumor growth and prolongation of survival. A, tumor size of subcutaneous tumors after MUC1-B16F10 cells challenge. +, death. B, survival of vaccinated KO mice. Survival curves were generated by Kaplan-Meier method and assessed by log-rank test ($P = 0.003$). C, Ab production against other unknown TAAs, assessed by Western blot analysis. Single arrow, the band of MUC1 protein at 150 kDa; arrowheads, the band of unknown TAAs from PANC1 cells. Representative data of five experiments with similar results.

(Fig. 5A and B). Tumor growth in mice vaccinated with α-gal PANC1 or parental PANC1 was monitored (Fig. 5A). Tumors in mice vaccinated with parental PANC1 doubled their sizes every 3 to 7 days and reached the maximum size of ~980 mm^2 within 22 to 25 days. For tumors in mice treated with α-gal PANC1, they continued to grow in nonvaccinated α1,3GT KO mice but displayed a much slower growth rate than most parental PANC1–treated KO mice. Tumors reached the size of 200 mm^2 within 20 to 36 days, whereas tumors in mice treated with parental PANC1 vaccines grew to a similar size within 12 to 14 days (Fig. 5A).

The beneficial effects of α-gal PANC1 vaccines were further shown in the prolongation of survival after tumor challenge. As shown in Fig. 5B, the mean survival time of KO mice treated with α-gal PANC1 was significantly prolonged (41.4 ± 10.4 d) compared with that of parental PANC1 vaccine (21.1 ± 10.5 d; $P = 0.003$; Fig. 5B).

α-gal PANC1 vaccines induce Ab production against MUC1 protein and other unknown tumor antigens

To understand the induced Ab response for other tumor antigens, the presence of immunostained PANC1 proteins was investigated by Western blots with mice serum before and after vaccination. As shown in Fig. 5C, sera from α1,3GT nonimmunized or pig kidney fragment–immunized KO mice did not contain any Ab that bound to MUC1 protein, and displayed only several nonspecific bands. Sera obtained from *α1,3GT* KO mice vaccinated with parental PANC1 also did not display obvious bands that were reflected by anti-MUC1 Ab. No detectable differences in these blot profiles were observed before and after parental PANC1 vaccine. In contrast, sera from α-gal PANC1–vaccinated *α1,3GT* KO mice were positive for Abs that bound to not only MUC1 protein but also different immunogenic proteins in PANC1 cells. These findings indicate that the expression of α-gal epitopes on TAAs in PANC1 cells can upregulate its immunogenicity and can induce the production of Abs against TAAs, including MUC1 and various tumor proteins.

Vaccination with α-gal PANC1 can effectively elicit immune response against pancreatic cancer stem cells

To assess Ab production against parental PANC1 cells, cells were stained with sera from vaccinated KO mice. As shown in Fig. 6A, sera from α-gal PANC1–vaccinated KO mice more strongly interacted with PANC1 cells than those from parental PANC1–vaccinated mice, as judged by the mean fluorescence intensity. Next, we confirmed that the subpopulation of pancreatic cancer stem cells expressed CD44, CD24, and ESA in parental PANC1 cells. Flow cytometric quantification (Fig. 6B) showed that 82.8% to 87.0% of parental PANC1 cells expressed CD44, 72.8% to 75.6% expressed CD24, and 91.4% to 93.8% expressed ESA. Examination of the expression of multiple surface markers showed 70.4% of PANC1 cells were CD44+CD24+ and 82.4% were CD44+ESA+. We isolated PANC1 cells with $CD44^+CD24^+$ phenotype by magnetic beads as described in Materials and Methods to investigate Ab production against both pancreatic cancer stem cells (i.e., binding PANC1 cells with beads)

Published OnlineFirst June 8, 2010; DOI:10.1158/0008-5472.CAN-09-4313

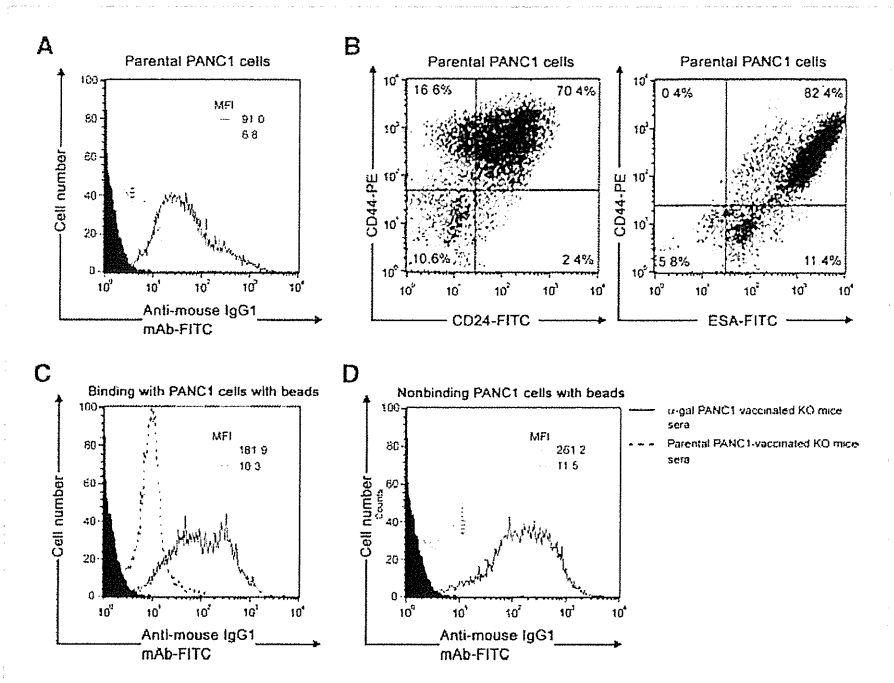

Figure 6. Production of Abs against cancer stem cells assessed by flow cytometry assay. A, production of anti-PANC1 Ab in sera from vaccinated KO mice. Closed histogram, unstained cells; open histogram, stained cells with sera from vaccinated KO mice. B, quantification of $CD44^+CD24^+$ PANC1 cells and $CD44^+ESA^+$ PANC1 cells. C, production of anti–$CD44^+CD24^+$ PANC1 Ab in sera from vaccinated KO mice. Closed histogram, unstained cells; open histogram, stained cells with sera from vaccinated KO mice. D, production of anti-$CD44^-CD24^-$ PANC1 Ab in sera from vaccinated KO mice. Closed histogram, unstained cells; open histogram, stained cells with sera from vaccinated KO mice. Representative data of five experiments with similar results.

and differentiated pancreatic cancer cells (i.e., nonbinding cells with beads). A strong Ab production against both pancreatic cancer stem cells and differentiated pancreatic cancer cells was effectively elicited by vaccination with α-gal PANC1 cells; however, vaccination with parental PANC1 cells did not induce any immune response against each subpopulation (Fig. 6C and D).

Discussion

Development of immunotherapy for pancreatic cancer is necessary to improve the poor prognosis associated with this disease. In this study, we showed the *in vitro* and *in vivo* effectiveness of immunotherapy through vaccination, with a resultant increase in immunogenicity of α-gal MUC1, and showed that repeated vaccination with α-gal PANC1 elicited the production of anti-MUC1 Ab as well as the generation of an effective cytotoxic T lymphocyte (CTL) response against the MUC1 molecule. Although MUC1 protein is a potential target for the immunotherapy of pancreatic cancer, vaccination against a single antigen is disadvantageous because it is not clear which antigens, including MUC1, have the potential to induce effective antitumor immune responses. In addition, immunity against various antigens is expected to be effective in heterogeneous cell populations of tumors.

Therefore, the use of unfractionated TAAs in the form of tumor cell lysates or whole cancer cells circumvented these disadvantages as described above. In this study, we used vaccination with whole cancer cells, and the immunogenicity of well-characterized as well as uncharacterized multiple TAAs contained in cancer cells was upregulated by α-gal epitopes; and thus, these TAAs would be effectively internalized by APC, which phagocytose-vaccinating tumor cells opsonized by anti-Gal. Multiple TAAs can be presented to T cells by both MHC class I and class II pathways, ultimately leading to polyclonal expansion of both B and T cells. In this study, whereas the sera obtained from parental PANC1–vaccinated KO mice failed to produce both anti-MUC1 Ab and anti–unknown TAA Abs, those from α-gal PANC1–vaccinated KO mice contained several Abs that bound to not only MUC1 protein but also different unknown TAAs. Future studies are required to identify and characterize these unknown molecules as novel TAAs for immunotherapy of pancreatic cancer. For the development of an effective immunotherapy of pancreatic cancer, we proposed that tumor cell lysate is a suitable source of tumor antigens because it contains several known as well as unknown antigens that could elicit an antitumor immune response.

Recently, the existence of cancer stem cells was confirmed in acute myelogenous leukemia and was subsequently verified also in breast cancer and brain tumors (39, 40). Putative pancreatic cancer stem cells express CD44, CD24, and ESA, which are glycoprotein marker molecules that can be used to identify cancer stem cells (28–48). In the present study, sera obtained from α-gal PANC1–vaccinated KO mice produced anti–$CD44^+CD24^+$ PANC1 Ab, but those from parental PANC1–vaccinated KO mouse were negative for anti–$CD44^+24^+$ PANC1 Ab. These results suggest that the buildup of α-gal epitopes on carbohydrates of cancer stem cell markers, thus

Published OnlineFirst June 8, 2010; DOI:10.1158/0008-5472.CAN-09-4313

allowing these molecules to be internalized by APC, is a novel strategy for treatment of cancer stem cells, including pancreatic cancer stem cells.

Tumor lysate is a suitable material for vaccination because it contains not only differentiated cancer cells but also cancer stem cell population. Because the number of cancer stem cells is small, it is difficult to induce immune response against cancer stem cells by standard vaccination with tumor cell lysates. In contrast, vaccination with tumor lysate enzymatically engineered to express α-gal epitopes might result in elicitation of immune response toward these cancer stem cells because putative pancreatic cancer stem cells express glycoprotein marker molecules that can identify cancer stem cells (28, 40, 46). Accordingly, the α-gal epitopes could be synthesized on the carbohydrates of both TAAs and stem cell markers, allowing these molecules to be internalized by APC.

Overall, the anti-Gal–mediated *in situ* targeting of immunizing tumor cells to APC might provide the immune system with the opportunity to be activated effectively by several TAAs, including MUC1 in tumor cells. Furthermore, novel approaches using vaccines of α-gal epitope–expressing pancreatic cancer cells are anticipated to induce immune response against not only differentiated cancer cells but also cancer stem cells, and may lead to cure pancreatic cancer.

Disclosure of Potential Conflicts of Interest

No potential conflicts of interest were disclosed.

Acknowledgments

We thank Prof. Uri Galili (University of Massachusetts Medical School, Worcester, MA) for generously providing the α1,3GT KO mice, Prof. M. Oka and Dr. S. Hazama for kindly providing plasmids encoding the *MUC1* gene, Dr. H. Ogawa for generously providing plasmids encoding the murine *α1,3GT* gene, K. Moriwaki for the helpful review of the manuscript, and Dr. Issa for the careful editing of the manuscript.

Grant Support

Suzuken Memorial Foundation of Japan Grants to MT.

The costs of publication of this article were defrayed in part by the payment of page charges. This article must therefore be hereby marked *advertisement* in accordance with 18 U.S.C. Section 1734 solely to indicate this fact.

Received 11/26/2009; revised 03/19/2010; accepted 04/13/2010; published OnlineFirst 06/08/2010.

References

1. Jemal A, Siegel R, Ward E, Hao Y, Xu J, Thun MJ. Cancer statistics. CA Cancer J Clin 2009;59:225–49.
2. Cameron JL, Riall TS, Coleman J, et al. One thousand consecutive pancreaticoduodenectomies. Ann Surg 2006;244:10–5.
3. Ueno H, Kosuge T, Matsuyama Y, et al, Japanese Study Group of Adjuvant Therapy for Pancreatic Cancer. A randomised phase III trial comparing gemcitabine with surgery-only in patients with resected pancreatic cancer. Br J Cancer 2009;101:908–15.
4. Jerome KR, Barnd DL, Bendt KM, et al. Cytotoxic T-lymphocytes derived from patients with breast adenocarcinoma recognize an epitope present on the protein core of a mucin molecule preferentially expressed by malignant cells. Cancer Res 1991;51:2908–16.
5. Hinoda Y, Ikematsu Y, Horinochi M, et al. Increased expression of MUC1 in advanced pancreatic cancer. J Gastroenterol 2003;38:1162–6.
6. Taylor-Papadimitriou J, Burchell J, Miles DW. MUC1 and cancer. Biochim Biophys Acta 1999;1455:301–13.
7. Gendler SJ. MUC1, the renaissance molecule. J Mammary Gland Biol Neoplasia 2001;6:339–53.
8. Masaki Y, Oka M, Ogura Y, et al. Sialylated MUC1 mucin expression in normal pancreas, benign pancreatic lesions, and pancreatic ductal adenocarcinoma. Hepatogastroenterology 1999;46:2240–5.
9. Schuman JT, Grinstead JS, Apostolopoulos V, Campbell AP. Structural and dynamic consequences of increasing repeats in a MUC1 peptide tumor antigen. Biopolymers 2005;77:107–20.
10. Lepisto AJ, Moser AJ, Zeh H, et al. A phase I/II study of a MUC1 peptide pulsed autologous dendritic cell vaccine as adjuvant therapy in patients with resected pancreatic and biliary tumors. Cancer Ther 2008;6:955–64.
11. Loveland BE, Zhao A, White S, et al. Mannan-MUC1-pulsed dendritic cell immunotherapy: a phase I trial in patients with adenocarcinoma. Clin Cancer Res 2006;12:869–77.
12. Rong Y, Jin D, Wu W, et al. Induction of protective and therapeutic anti-pancreatic cancer immunity using a reconstructed MUC1 DNA vaccine. BMC Cancer 2009;9:191.
13. Danielczyk A, Stahn R, Faulstich D, et al. PankoMab: a potent new generation anti-tumour MUC1 antibody. Cancer Immunol Immunother 2006;55:1337–47.
14. Goldberger O, Volovitz I, Machlenkin A, Vadai E, Tzehoval E, Eisenbach L. Exuberated numbers of tumor-specific T cells result in tumor escape. Cancer Res 2008;68:3450–7.
15. Khong HT, Restifo NP. Natural selection of tumor variants in the generation of "tumor escape" phenotypes. Nat Immunol 2002;3:999–1005.
16. Galili U, Tibell A, Samuelsson B, Rydberg L, Groth CG. Increased anti-Gal activity in diabetic patients transplanted with fetal porcine islet cell clusters. Transplantation 1995;59:1549–56.
17. Galili U, Rachmilewitz EA, Peleg A, Flechner I. A unique natural human IgG antibody with anti-α-galactosyl specificity. J Exp Med 1984;160:1519–31.
18. Davin JC, Malaise M, Foidart J, Mahieu P. Anti-α-galactosyl antibodies and immune complexes in children with Henoch-Schönlein purpura or IgA nephropathy. Kidney Int 1987;31:1132–9.
19. Galili U, Mandrell RE, Hamadeh RM, Shohet SB, Griffiss JM. Interaction between human natural anti-α-galactosyl immunoglobulin G and bacteria of the human flora. Infect Immun 1988;56:1730–7.
20. Galili U, Wigglesworth K, Abdel-Motal UM. Intratumoral injection of α-gal glycolipids induces xenograft-like destruction and conversion of lesions into endogenous vaccines. J Immunol 2007;178:4676–87.
21. Abdel-Motal UM, Wigglesworth K, Galili U. Intratumoral injection of α-gal glycolipids induces a protective anti-tumor T cell response which overcomes Treg activity. Cancer Immunol Immunother 2009;58:1545–56.
22. Abdel-Motal UM, Wigglesworth K, Galili U. Mechanism for increased immunogenicity of vaccines that form *in vivo* immune complexes with the natural anti-Gal antibody. Vaccine 2009;27:3072–82.
23. Galili U, Clark MR, Shohet SB, Buehler J, Macher BA. Evolutionary relationship between the natural anti-Gal antibody and the Gal α 1→3Gal epitope in primates. Proc Natl Acad Sci U S A 1987;84:1369–73.
24. Galili U, Shohet SB, Kobrin E, Stults CL, Macher BA. Man, apes, and Old World monkeys differ from other mammals in the expression of α-galactosyl epitopes on nucleated cells. J Biol Chem 1988;263:17755–62.
25. Galili U, Swanson K. Gene sequences suggest inactivation of

Published OnlineFirst June 8, 2010; DOI:10.1158/0008-5472.CAN-09-4313

α-1,3-galactosyltransferase in catarrhines after the divergence of apes from monkeys. Proc Natl Acad Sci U S A 1991;88:7401–4.
26. Tanemura M, Yin D, Chong AS, Galili U. Differential immune responses to α-gal epitopes on xenografts and allografts: implications for accommodation in xenotransplantation. J Clin Invest 2000;105: 301–10.
27. Tanemura M, Saga A, Kawamoto K, et al. *In vitro* and *in vivo* prevention of human CD8+ CTL-mediated xenocytotoxicity by pig c-FLIP expression in porcine endothelial cells. Am J Transplant 2008;8: 288–97.
28. Li C, Heidt DG, Dalerba P, et al. Identification of pancreatic cancer stem cells. Cancer Res 2007;67:1030–7.
29. LaTemple DC, Abrams JT, Zhang SY, Galili U. Increased immunogenicity of tumor vaccines complexed with anti-Gal: studies in knockout mice for α1,3galactosyltransferase. Cancer Res 1999;59: 3417–23.
30. Tanemura M, Ogawa H, Yin DP, Chen ZC, DiSesa VJ, Galili U. Elimination of anti-Gal B cells by α-Gal ricin1. Transplantation 2002;73:1859–68.
31. Yuan Z, Wong S, Borrelli A, Chung MA. Down-regulation of MUC1 in cancer cells inhibits cell migration by promoting E-cadherin/catenin complex formation. Biochem Biophys Res Commun 2007;362:740–6.
32. Sipos B, Möser S, Kalthoff H, Török V, Löhr M, Klöppel G. A comprehensive characterization of pancreatic ductal carcinoma cell lines: towards the establishment of an *in vitro* research platform. Virchows Arch 2003;442:444–52.
33. Gorelik E, Duty L, Anaraki F, Galili U. Alterations of cell surface carbohydrates and inhibition of metastatic property of murine melanomas by α 1,3 galactosyltransferase gene transfection. Cancer Res 1995;55:4168–73.
34. Ogawa H, Galili U. Profiling terminal N-acetyllactosamines of glycans on mammalian cells by an immuno-enzymatic assay. Glycoconj J 2006;23:663–74.
35. Galili U, LaTemple DC, Radic MZ. A sensitive assay for measuring α-Gal epitope expression on cells by a monoclonal anti-Gal antibody. Transplantation 1998;65:1129–32.
36. Mueller MT, Hermann PC, Witthauer J, et al. Combined targeted treatment to eliminate tumorigenic cancer stem cells in human pancreatic cancer. Gastroenterology 2009;137:1102–13.
37. Ohdan H, Yang YG, Shimizu A, Swenson KG, Sykes M. Mixed chimerism induced without lethal conditioning prevents T cell- and anti-Gal α 1,3Gal-mediated graft rejection. J Clin Invest 1999;104: 281–90.
38. Hosoi A, Takeda Y, Furuichi Y, et al. Memory Th1 cells augment tumor-specific CTL following transcutaneous peptide immunization. Cancer Res 2008;68:3941–9.
39. Al-Hajj M, Wicha MS, Benito-Hernandez A, Morrison SJ, Clarke MF. Prospective identification of tumorigenic breast cancer cells. Proc Natl Acad Sci U S A 2003;100:3983–8.
40. Singh SK, Hawkins C, Clarke ID, et al. Identification of human brain tumour initiating cells. Nature 2004;432:396–401.
41. Galili U, LaTemple DC. Natural anti-Gal antibody as a universal augmenter of autologous tumor vaccine immunogenicity. Immunol Today 1997;18:281–5.
42. LaTemple DC, Galili U. Adult and neonatal anti-Gal response in knock-out mice for α1,3galactosyltransferase. Xenotransplantation 1998;5:191–6.
43. Thall AD, Malý P, Lowe JB. Oocyte Gal α 1,3Gal epitopes implicated in sperm adhesion to the zona pellucida glycoprotein ZP3 are not required for fertilization in the mouse. J Biol Chem 1995;270:21437–40.
44. LaTemple DC, Henion TR, Anaraki F, Galili U. Synthesis of α-galactosyl epitopes by recombinant α1,3galactosyl transferase for opsonization of human tumor cell vaccines by anti-galactose. Cancer Res 1996;56:3069–74.
45. Pandey P, Kharbanda S, Kufe D. Association of the DF3/MUC1 breast cancer antigen with Grb2 and the Sos/Ras exchange protein. Cancer Res 1995;55:4000–3.
46. Reya T, Morrison SJ, Clarke MF, Weissman IL. Stem cells, cancer, and cancer stem cells. Nature 2001;414:105–11.
47. Lee CJ, Dosch J, Simeone DM. Pancreatic cancer stem cells. J Clin Oncol 2008;26:2806–12.
48. Huang P, Wang CY, Gou SM, et al. Isolation and biological analysis of tumor stem cells from pancreatic adenocarcinoma. World J Gastroenterol 2008;14:3903–7.

Journal of Surgical Research ■, 1–7 (2010)
doi:10.1016/j.jss.2010.07.023

Effects of Pegylated Interferon α2b on Metastasis of Hepatocellular Carcinoma[1]

Yusuke Arakawa, M.D., Mitsuo Shimada, M.D., F.A.C.S.,[2] Tohru Utsunomiya, M.D., Satoru Imura, M.D., Yuji Morine, M.D., and Tetsuya Ikemoto, M.D.

Department of Surgery, Institute of Health Biosciences, The University of Tokushima, Tokushima, Japan

Submitted for publication May 15, 2010

Objective. **Interferon (IFN) has an anti-tumor activity in hepatocellular carcinoma (HCC) *via* anti-angiogenesis and induction of apoptosis. We have previously reported anti-metastatic effects of IFN combined chemotherapy on the outcome of HCC patients. The aim of this study was to investigate anti-metastatic effects of IFN.**

Methods. **In vitro, pegylated interferon α2b (PEG-IFN-α2b) was administered to mouse MH134 cells (mouse HCC cell line, MH134), and anti-implantation effects were examined by evaluating the inhibition of cell invasion and cell proliferation. Expressions of vascular endothelial growth factor (VEGF) mRNA were also measured. *In vivo*, PEG-IFN-α2b was subcutaneously administered into MH134 cells and tumor growth was evaluated. In distant metastasis models, PEG-IFN-α2b was subcutaneously administered and MH134 cells were injected into the spleen. The number of liver metastases and microvessel densities (MVD) were counted.**

Results. ***In vitro*, the proliferation of MH134 cells was significantly suppressed by PEG-IFN-α2b dose-dependently. MH134 cells added with PEG-IFN-α2b exhibited significantly lower levels of invasion potential. *In vivo*, tumor size in mice treated with PEG-IFN-α2b significantly suppressed compared with control mice (mean 0.5 *versus* 5.0 cm, in diameter, $P < 0.05$) and also decreased number of liver metastases (19.3 *versus* 6.0, $P < 0.05$). Moreover, PEG-IFN-α2b significantly suppressed angiogenesis compared with the control.**

Conclusion. **PEG-IFN-α2b in itself had remarkable anti-metastatic effects *via* inhibition of angiogenesis and cell adhesions.** © 2010 Published by Elsevier Inc.

Key Words: **hepatocellular carcinoma; metastasis; interferon.**

INTRODUCTION

Hepatocellular carcinoma (HCC), which is the main type of primary liver cancer, is one of the most common and aggressive malignancies. Hepatic resection is the standard treatment for HCC; however, the survival rate is still low because of the high incidence of recurrence [1]. Especially the tumor portal vein thrombus is poor prognostic factor due to intra- and extra-hepatic metastasis [2]. HCC is not generally sensitive to chemotherapy. Recently, new chemotherapy has appeared and interferon (IFN) has an anti-tumor activity in HCC *via* anti-angiogenesis and induction apoptosis for primary liver lesion [3–5]. We have already reported anti-metastatic effects of IFN combined chemotherapy (CDDP+5-FU) on the outcome of HCC patients [6]. There are some reports demonstrating the inhibitory effects on HCC after IFN therapy alone [7, 8]. However, mechanisms of anti-metastatic effects of IFN for HCC are still unclear. Cancer metastasis is the hallmark of malignant tumors. The progressive metastasis of malignant tumors depends mainly on angiogenesis and cell adhesion [9–11]. The aim of this study is to investigate the effects of IFN inhibiting HCC proliferation and metastasis *via* angiogenesis and cell adhesions.

MATERIALS AND METHODS

Cell Line and Animals

MH134, a mouse hepatocellular carcinoma cell line, was moderately differentiated and grows in synergenic recipients in both solid and ascitic forms [12]. The cell lines were kindly provided from Cell

[1] A part of this study was presented in ASCO-GI, San Francisco, January 16–18, 2009.

[2] To whom correspondence and reprint requests should be addressed at Institute of Health Biosciences, Department of Surgery, The University of Tokushima Graduate School, 3-18-15 Kuramoto, Tokushima, 770-8503 Japan. E-mail: mshimada@clin.med.tokushima-u.ac.jp.

0022-4804/$36.00

Resource Center for Biomedical Research, Institute of Development, Aging, and Cancer, Tohoku University (Sendai, Japan).

Six-wk-old male C3H/HEN Crj mice were obtained from Charles River Laboratories (Kanagawa, Japan). Animals were provided with water and standard laboratory diet for at least 7 d before use. Throughout the experiment, the animals were maintained behind barriers under controlled conditions and had free access to tap water and food. The present study was conducted in compliance with the Division for Animal Research Resources, Institute of Health Biosciences, and the University of Tokushima. The experiments and procedures were approved by the Animal Care and Use Committee of the University of Tokushima.

Interferon

Pegylated IFN α2b (PEG-IFN-α2b) was kindly provided by Schering-Plough K.K. (Osaka, Japan). The specific activity of PEG-IFN-α2b was 6.4×10^7 IU/mg protein.

Experiment 1 (*In Vitro*) MTT Assay

PEG-IFN-α2b was added to MH134 cells and anti-proliferative effects were examined by evaluating 3-(4, 5-dimethyithiazol-2yl)-2,5-diphenyltetrazolium bromide (MTT) assay (Chemicon International Inc., Temecula, CA, USA). The cells were seeded on 96-well plates (Coster; Corning Inc., Tokyo, Japan), cultured for 24 h, and the culture medium was changed to a new medium with or without PEG-IFN-α2b (1×10^3, 1×10^4, 1×10^5 IU/mL). After culturing for 24, 48, 72, or 96 h, the number of viable cells was measured with absorbance meter (F-2500; Hitachi, Tokyo, Japan) by setting the wavelength at 570 nm [13].

Cell Invasion Assay

PEG-IFN-α2b was added to MH134 cells and anti-invasion effects were examined by evaluating cell invasion assay (Cultrex 96 Well BME Cell Invasion Assay). The assay kit was adapted to multiple formats so that cell invasion might be evaluated against different extracellular matrices; laminin 1, collagen 1, and collagen 4. The cells were seeded on 96-well plates, cultured for 24 h, and the culture medium was changed to a new medium with or without PEG-IFN-α2b (1×10^3, 1×10^4, 1×10^5 IU/mL). After culturing for 24 h, the number of viable cells was measured with absorbance meter (F-2500; Hitachi) by setting the wavelength at 520 nm [14].

Quantitative Real Time RT-PCR for VEGF and bFGF in HCC Cells

The mRNA expression levels of vascular endothelial growth factor (VEGF) and basic fibroblast growth factor (bFGF) were evaluated by quantitative real time reverse transcription polymerase chain reaction (RT-PCR). Total RNA was extracted from cultured MH134 cells in medium containing (1×10^3, 1×10^4, 1×10^5 IU/mL) PEG-IFN-α2b using RNeasy Mini Kit (Qiagen, Hilden, Germany). Quantitative real time RT-PCR was performed by using an ABI 7500 real-time PCR system (PE Applied Biosystems, Carlsbad, CA, USA). TaqMan gene expression systems (PE Applied Biosystems) for VEGF (assay ID Mm00437304) and bFGF (assay ID Mm01285715) were used for quantification of mRNA expression of the respective genes. To normalize, amplification of GAPDH (TaqMan ribosomal RNA control reagents, assay ID Rn9999916) was performed as an endogenous control.

Experiment 2 (*In Vivo*, Subcutaneous Injection Model)

The mice were divided into two groups; control group ($n = 10$) and IFN group ($n = 10$). Twenty-four hours before subcutaneous implantation of the MH134 cells (1×16^5 cells/mouse), IFN (1×10^3, 1×10^4, or 1×10^5 IU/body) was subcutaneously administered in each mouse. Tumor maximum diameter was measured in single direction using calipers 7 d after cell transplantation.

Experiment 3 (*in vivo*, Intrahepatic *Via* Portal Vein Metastasis Model) Intrahepatic and Portal Vein Metastasis Model (Splenic Injection Model)

Six-wk-old male C3H/HEN Crj mice were obtained from Charles River Laboratories, and were anesthetized with ether. A small upper-quadrant incision was made to expose the spleen. Using a 27-gauge needle, 1×10^5 cells/mouse was injected into the lower splenic pole. One week after splenic injection, the number of macroscopic metastases on the surface of the liver was counted [15]. Twenty-four hours before the splenic injection, IFN (1×10^3,1×10^4, or 1×10^5 IU/body) was subcutaneously administered in each mouse.

Quantification of Microvessel Density

Excised liver specimens were fixed in 10% formaldehyde and embedded in paraffin. Histologic study was performed on 4 μm sections stained with hematoxylin and eosin. Immunohistochemical staining was performed on 4 μm sections using the anti-mouse CD34 antibody (H-140; Santa Cruz Biotechnology, Inc., Santa Cruz, CA). Overnight incubation at 4°C with primary antibody and indirect immunoperoxidase staining with the avidin-biotin complex (DAKO, Glostrup, Denmark) and DAB Tablet (Wako Pure Chemical Industries, Ltd. Osaka, Japan) were applied for visualization of the antigens. Quantification of blood vessels was carried out as described previously [16]. Any brown-staining endothelial cell cluster distinct from adjacent microvessels, tumor cells, or other stromal cells was considered a single countable microvessel. Sections were examined at a magnification of $\times$400, and five fields were randomly chosen to determine the expression of CD34 by two pathologists who had no direct relation to this study. Expression of these proteins was evaluated as the number of positive staining cells.

Histology and Immunohistochemistry (ICAM and VCAM) in the HCC

Vascular cell adhesion molecule-1 (VCAM) and intercellular adhesion molecule-1 (ICAM) are expressed in the normal mouse hepatic sinusoid [17]. Excised liver specimens were fixed in 10% formaldehyde and embedded in paraffin. Histologic study was performed on 4 μm sections stained with hematoxylin and eosin. Immunohistochemical staining was performed on 4 μm sections using the anti-mouse ICAM antibody (10020-1-AP; ProteinTech Group, Inc., Chicago, IL) and anti-mouse VCAM antibody (sc-8304; Santa Cruz Biotechnology, Inc.). Overnight incubation at 4°C with primary antibody and indirect immunoperoxidase staining with the avidin-biotin complex (DAKO) and DAB Tablet (Wako Pure Chemical Industries, Ltd.) were applied for visualization of the antigens.

Statistical Analysis

All results were presented as mean ± standard deviation (SD). Student's t-test and Mann-Whitney U test were used for statistical analysis. P value < 0.05 was considered statistically significant.

RESULTS

MTT Assay

To evaluate the effect of PEG-IFN-α2b for MH134 cells, we performed MTT assay. Twenty-four hours after the

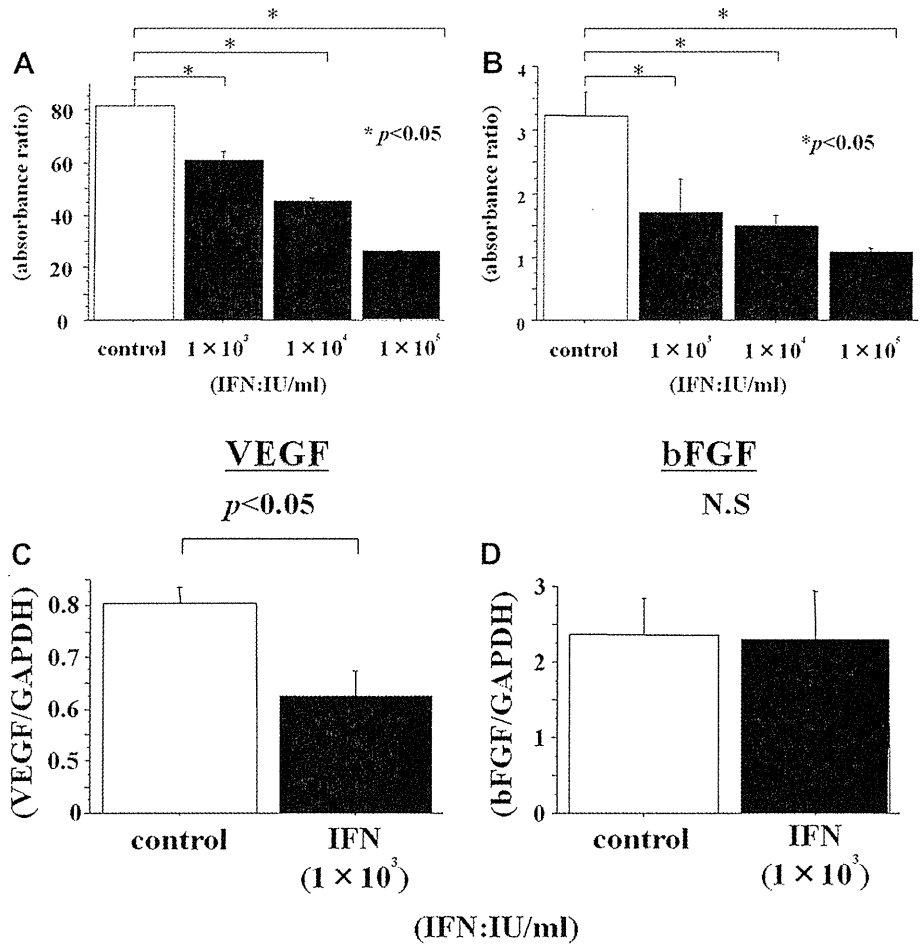

FIG. 1. (A) MTT assay showed antiproliferative effect of PEG-IFN-α2b. The proliferation of MH134 cells was suppressed dose-dependently ($P < 0.05$). (B) Invasion assay showed anti-invasive effect of PEG-IFN-α2b. The invasion of the matrigel-coated filters was suppressed dose-dependently ($P < 0.05$). (C) Expression of VEGF mRNA by quantitative real-time RT-PCR. (D) Expression of bFGF mRNA by quantitative real-time RT-PCR. *In vitro* inhibition of VEGF mRNA but not bFGF mRNA by PEG-IFN-α2b. mRNA was extracted in MH134 cells and those cells incubated in medium containing PEG-IFN-α2b ($P < 0.05$).

addition of PEG-IFN-α2b (1×10^3, 1×10^4, 1×10^5 IU/mL), the proliferation of MH134 cells was significantly suppressed by PEG-IFN-α2b dose-dependently compared with control group ($P < 0.05$, Fig. 1A).

Cell Invasion Assay

MH134 cells were examined in the invasion assay to determine if their ability to penetrate the reconstituted basement membrane matrigel. MH134 cells added with PEG-IFN-α2b (1×10^3, 1×10^4, 1×10^5 IU/mL) exhibited significantly lower levels of invasion potential (control *versus* PEG-IFN-α2b 1×10^3, 1×10^4, 1×10^5 IU/mL, mean 3.239 *versus* 1.707, 1.499, 1.047, Fig. 1B).

Quantitative Real Time-PCR for VEGF and bFGF in HCC Cells

Anti-angiogenic effects of PEG-IFN-α2b on MH134 cells by blocking the expression of VEGF and bFGF were studied. The expression of VEGF mRNA decreased in cells with PEG-IFN-α2b significantly ($P < 0.05$, Fig. 1C). The treatment with PEG-IFN-α2b resulted in a reduction of VEGF mRNA for 24 h. However, the expression of bFGF mRNA in the cells with PEG-IFN-α2b did not differ significantly compated with the control ($P > 0.05$, Fig. 1D).

Tumor Diameter

Dose-dependent suppression of tumor diameter was observed in mice receiving PEG-IFN-α2b. PEG-IFN-α2b significantly suppressed compared with control mice ($P < 0.05$, Fig. 2).

Liver Metastasis

Macroscopic metastasis of all mice could be seen on the surface of the liver. PEG-IFN-α2b significantly